Department of Mechanical Engineering

# Numerical crack nucleation and propagation analyses of bonded joints

Jarno Jokinen

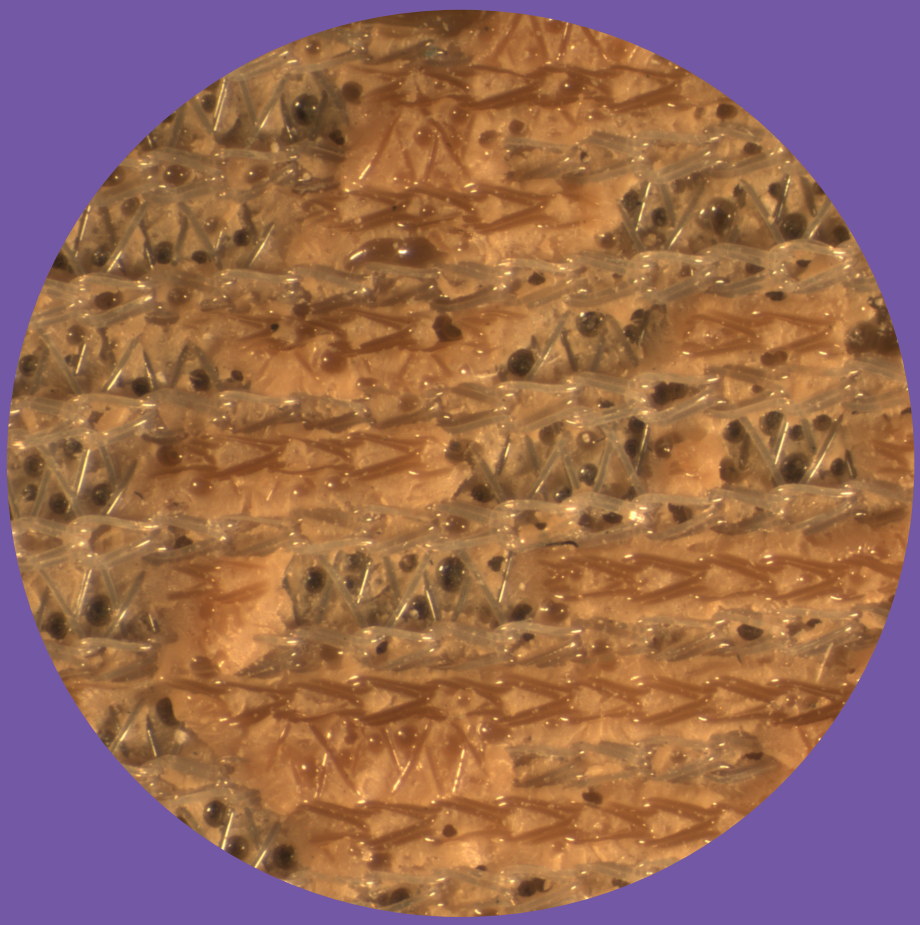

Aalto University

DOCTORAL DISSERTATIONS

Aalto University publication series
**DOCTORAL DISSERTATIONS** 212/2019

# Numerical crack nucleation and propagation analyses of bonded joints

**Jarno Jokinen**

A doctoral dissertation completed for the degree of Doctor of Science (Technology) to be defended, with the permission of the Aalto University School of Engineering, at a public examination held at the lecture hall K215 of the school on 22 November 2019 at 12.

**Aalto University**
**School of Engineering**
**Department of Mechanical Engineering**

**Supervising professor**
Prof. Olli Saarela, Aalto University, Finland

**Thesis advisor**
Prof. Mikko Kanerva, Tampere University, Finland

**Preliminary examiners**
Prof. Albert Turon, University of Girona, Spain
Prof. Adrian Orifici, Royal Melbourne Institute of Technology, Australia

**Opponent**
Prof. Pedro Camanho, University of Porto, Portugal

Aalto University publication series
**DOCTORAL DISSERTATIONS** 212/2019



ISBN 978-952-60-8824-2 (printed)
ISBN 978-952-60-8825-9 (pdf)
ISSN 1799-4934 (printed)
ISSN 1799-4942 (pdf)
http://urn.fi/URN:ISBN:978-952-60-8825-9

Unigrafia Oy
Helsinki 2019

Finland

NORDIC SWAN ECOLABEL
Printed matter
4041-0619

Aalto University

# Abstract

Aalto University, P.O. Box 11000, FI-00076 Aalto www.aalto.fi

**Author**
Jarno Jokinen

**Name of the doctoral dissertation**
Numerical crack nucleation and propagation analyses of bonded joints

**Publisher** School of Engineering

**Unit** Department of Mechanical Engineering

**Series** Aalto University publication series DOCTORAL DISSERTATIONS 212/2019

**Field of research** Aeronautical Engineering

**Manuscript submitted** 17 May 2019 **Date of the defence** 22 November 2019

**Permission for public defence granted (date)** 23 October 2019 **Language** English

☐ **Monograph** ☒ **Article dissertation** ☐ **Essay dissertation**

**Abstract**

Delamination and debonding are typical interface failures that may endanger the structural integrity of laminated and adhesively bonded structures. Two numerical fracture analysis methods, the virtual crack closure technique (VCCT) and the cohesive zone model (CZM), are commonly used tools to criticality analyse such failures. The objective of this thesis work is to study the limitations of the VCCT and the CZM and to extend their applicability.

The work consists of four case studies. The first two studies focus on the VCCT that is typically used in crack propagation analyses when material plasticity can be ignored. The possibility to use the method in analyses of adhesively bonded joints with a yielding adhesive and with yielding adherends is studied with analysis cases of double cantilever beam (DCB) and wedge peel test specimens. The experimental results provided a reference for the analyses. In the third study, a method combining the CZM and the VCCT is developed for crack nucleation and propagation analyses. The applicability of the method is studied with analyses of the DCB test. The final study concentrates on fracture models of hybrid laminates under mixed-mode loading and thermal stresses. A hybrid laminate cracked lap shear (CLS) specimen was analysed in the study by using the VCCT, the CZM and their combination.

The thesis work indicates that the VCCT is a feasible analysis method for crack propagation analyses of a DCB specimen with a yielding adhesive. Comparing to analytical (initial crack length) solutions, the VCCT also improves correlation with experimental data when plasticity exists in the adherends of a wedge peel test specimen. The developed combined CZM-VCCT method is feasible for analysing the crack nucleation and propagation phases of the DCB specimen. The combined method is also able to estimate crack onset for a hybrid laminate CLS specimen. The hybrid laminate study further indicates that the CZM is feasible and the VCCT is unfeasible for analyses of hybrid laminates with thermal loading.

**Keywords** VCCT, CZM, delamination

**ISBN (printed)** 978-952-60-8824-2 **ISBN (pdf)** 978-952-60-8825-9

**ISSN (printed)** 1799-4934 **ISSN (pdf)** 1799-4942

**Location of publisher** Helsinki **Location of printing** Helsinki **Year** 2019

**Pages** 135 **urn** http://urn.fi/URN:ISBN:978-952-60-8825-9

**Tekijä**
Jarno Jokinen

**Väitöskirjan nimi**
Numeerinen särön synnyn ja kasvun analysointi liimaliitoksessa ja komposiittilaminaatissa

**Julkaisija** Insinööritieteiden korkeakoulu

**Yksikkö** Konetekniikan laitos

**Sarja** Aalto University publication series DOCTORAL DISSERTATIONS 212/2019

**Tutkimusala** Lentotekniikka

**Käsikirjoituksen pvm** 17.05.2019 **Väitöspäivä** 22.11.2019

**Väittelyluvan myöntämispäivä** 23.10.2019 **Kieli** Englanti

☐ **Monografia** ☒ **Artikkeliväitöskirja** ☐ **Esseeväitöskirja**

**Tiivistelmä**

Delaminaatiot ja liimaliitosten murtumiset ovat yleisiä rajapintavaurioita, jotka voivat merkittävästi alentaa rakenteiden kuormankantokykyä. Vaurioiden kriittisyyttä arvioidaan tyypillisesti numeerisilla analyysimenetelmillä, joista kaksi yleisintä ovat virtuaalisen särön sulkemismenetelmä (Virtual Crack Closure Technique, VCCT) ja koheesioelementit (Cohesive Zone Modelling, CZM). Väitöskirjan tavoitteena on tarkastella kyseisten menetelmien rajoituksia ja laajentaa niiden käytettävyyttä.

Työ jakautuu neljään osatutkimukseen. Kahdessa ensimmäisessä tarkastelun kohteena on VCCT-menetelmä, jonka käyttö rajoittuu tavallisesti elastisten rakenteiden särönkasvutarkasteluihin. Tutkimuksessa selvitetään menetelmän toimivuutta, kun liimaliitoksen liimassa tai liimattavissa kappaleissa esiintyy plastisuutta. Toimivuutta tarkastellaan analysoimalla standardien mukaisia liimakoekappaleita ja vertaamalla laskennan tuloksia kokeissa mitattuihin tuloksiin. Kolmannessa osatutkimuksessa tarkastelun kohteena on CZM- ja VCCT-menetelmien yhdistelmä. Työssä kehitetyssä menetelmässä koheesioelementtejä käytetään särön muodostumisen analysointiin ja VCCT:tä särön kasvun analysointiin. Menetelmän toimivuutta tarkastellaan vertaamalla standardikoekappaleen laskentatuloksia koetuloksiin ja muiden laskentamenetelmien antamiin tuloksiin. Väitöskirjan viimeisessä osatutkimuksessa tarkastellaan särön syntyä ja kasvua lämpöjännitysten ja mekaanisen kuorman rasittamassa, hybridilaminaatista valmistetussa koekappaleessa. CZM-, VCCT- ja yhdistelmämenetelmillä laskettujen tulosten hyvyyttä arvioidaan vertaamalla niitä koetuloksiin.

Tutkimus osoittaa, että VCCT-menetelmä soveltuu tarkastelutapausta vastaavien liimaliitosten analyysiin myös silloin, kun liima-aine myötää kuormituksen vaikutuksesta. VCCT antaa myös analyyttisiin laskentamenetelmiin verrattuna paremman tuloksen säröpituudelle, kun tarkastelun kohteena on koekappale, jossa liimatut metallilevyt myötävät. Kehitetyn CZM-VCCT yhdistelmämenetelmän todetaan antavan kokeita vastaavia tuloksia tarkastellulle koekappaleelle eri särön kasvun vaiheissa. Yhdistelmämenetelmällä on mahdollista arvioida myös särön muodostumista hybridilaminaatista valmistetussa, lämpöjännitysten ja mekaanisen kuorman rasittamassa koekappaleessa. Myös CZM-menetelmä todetaan tähän tarkoitukseen soveltuvaksi, kun taas VCCT-menetelmällä ei voida analysoida kyseisen tyyppistä kuormitustapausta.

**Avainsanat** VCCT, koheesioelementit, delaminaatio

**ISBN (painettu)** 978-952-60-8824-2 **ISBN (pdf)** 978-952-60-8825-9

**ISSN (painettu)** 1799-4934 **ISSN (pdf)** 1799-4942

**Julkaisupaikka** Helsinki **Painopaikka** Helsinki **Vuosi** 2019

**Sivumäärä** 135 **urn** http://urn.fi/URN:ISBN:978-952-60-8825-9

# Acknowledgements

My dissertation has been carried out in the department of Mechanical Engineering at Aalto University and in the faculty of Engineering and Natural Sciences in Tampere University. It was funded by the Finnish Defence Forces Logistics Command, and the Ministry of Education Finland National Graduate School in Engineering Mechanics. The financial support is gratefully acknowledged. The CSC – IT Center for Science Ltd. is acknowledged for providing Abaqus and analyses resources.

Firstly, I want to acknowledge my supervisor, Professor Olli Saarela. He offered me the opportunity to do the work and provided valuable comments for the articles and thesis. Secondly, I would like to express my gratitude to the instructor, Professor Mikko Kanerva. His encouragement and support have been priceless. I also want to acknowledge Markus Wallin for all the support he gave me during the thesis work and beyond. Further, I wish to thank my colleagues in Aalto and Tampere, especially Jarkko Aakkula and Tuomas Pärnänen. Finally, I wish to thank Ari Kivistö from the Finnish Defence Forces Logistics Command and Reijo Lindgren from Dassault Systems.

I want to acknowledge my thesis pre-examiners Professor Albert Turon and Professor Adrian Orifici, and my opponent Professor Pedro Camanho for their valuable work.

Finally, I would like to express my deepest gratitude to my parents, my brother Markus, Annina, my relatives and friends. Sometimes words are not enough for expressing thanks.

Espoo, 1 October 2019
Jarno Jokinen

# Contents

# List of Abbreviations and Symbols

### Symbols

| | |
|---|---|
| $A$ | area |
| $a$ | crack length |
| $B, b$ | width |
| $E$ | Young's modulus |
| $F$ | force |
| $f$ | fracture criterion |
| $G$ | energy release rate |
| $h$ | thickness |
| $K$ | cohesive stiffness |
| $L$ | length |
| $M$ | moment |
| $N$ | load-block correction |
| $n$ | hardening exponent |
| $P$ | force |
| $R$ | fracture toughness |
| $r$ | radius |
| $T$ | temperature |
| $u, v, w$ | displacement |
| $U, W$ | energy |
| $X, Y, Z$ | force |
| $Y$ | wedge thickness |
| $\alpha$ | yield offset |

| | |
|---|---|
| $\Delta$ | crack-length correction |
| $\delta$ | separation |
| $\varepsilon$ | strain |
| $\sigma$ | stress |
| $\tau$ | stress |
| $\psi$ | mode-mixity ($\tan^{-1}(K_{II}/K_{I})$) |

**Sub-indexes**

| | |
|---|---|
| a | adhesive |
| C | critical |
| l | lap |
| p | plastic |
| s | strap |
| I, II, III | fracture mode |

**Abbreviations**

| | |
|---|---|
| BJ | butt joint |
| CFRP | carbon fibre reinforced plastic |
| CLS | cracked lap shear |
| CZM | cohesive zone model |
| DCB | double cantilever beam |
| EDT | energy derivative technique |
| ENF | end-notched flexure |
| EP | elastic-plastic |
| EPFM | elastic-plastic fracture mechanics |
| ERR | energy release rate |
| FE | finite element |
| LEFM | linear elastic fracture mechanics |
| VCCT | virtual crack closure technique |

# List of Publications

This doctoral dissertation consists of a summary and of the following publications, which are referred to in the text by their numerals.

**1.** Jokinen, Jarno; Wallin, Markus; Saarela, Olli. 2015. Applicability of VCCT in mode I loading of yielding adhesively bonded joints – a case study. Elsevier. International Journal of Adhesion and Adhesives, volume 62, pages 85–91. ISSN 0143-7496. http://dx.doi.org/10.1016/j.ijadhadh.2015.07.004.

**2.** Aakkula, Jarkko; Jokinen, Jarno; Saarela, Olli; Tervakangas, Sanna. 2016. Testing and modelling of DIARC plasma coated elastic–plastic steel wedge specimens. Elsevier. International Journal of Adhesion and Adhesives, volume 68, pages 219–228. ISSN 0143-7496. http://dx.doi.org/10.1016/j.ijadhadh.2016.03.024.

**3.** Jokinen, Jarno; Kanerva, Mikko; Wallin, Markus; Saarela, Olli. 2019. The simulation of a double cantilever beam test using the virtual crack closure technique with the cohesive zone modelling. Elsevier. International Journal of Adhesion and Adhesives, volume 88, pages 50–58. ISSN 0143-7496. https://doi.org/10.1016/j.ijadhadh.2018.10.015.

**4.** Jokinen, Jarno; Kanerva, Mikko. 2017. Analysis of cracked lap shear testing of tungsten-CFRP hybrid laminates. Elsevier. Engineering Fracture Mechanics, volume 175, pages 184–200. ISSN 0013-7944. https://doi.org/10.1016/j.engfracmech.2017.01.029.

**5.** Jokinen, Jarno; Kanerva, Mikko. 2019. Simulation of delamination growth at CFRP-tungsten aerospace laminates using VCCT and CZM modelling techniques. Springer. Applied Composite Materials, volume 26, pages 709-721. ISSN 1573-4897. https://doi.org/10.1007/s10443-018-9746-5.

# Author's Contribution

**Publication 1:** Applicability of VCCT in mode I loading of yielding adhesively bonded joints – a case study

The author performed the finite element analysis, interpreted the results and wrote the manuscript. Wallin performed the experiments. Wallin and Saarela contributed to the manuscript writing in terms of conceptualisation.

**Publication 2:** Testing and modelling of DIARC plasma coated elastic–plastic steel wedge specimens

The author was responsible for the material model and VCCT model, and performed the finite element analysis. The author contributed to the manuscript writing in terms of the finite element analysis. Aakkula designed and performed the experiments, interpreted the results and wrote the manuscript. Saarela contributed to the manuscript and provided valuable comments and suggestions. Tervakangas performed DIARC coating preparation and contributed to the manuscript regarding the coating method.

**Publication 3:** The simulation of a double cantilever beam test using the virtual crack closure technique with the cohesive zone modelling

The author performed the finite element analysis. The author and Kanerva wrote the manuscript. Wallin performed the experiments. Wallin and Saarela contributed to the manuscript and provided valuable comments and suggestions.

**Publication 4:** Analysis of cracked lap shear testing of tungsten-CFRP hybrid laminates

The author performed all the finite element analyses. Kanerva performed the experiments. The author and Kanerva wrote the manuscript.

**Publication 5:** Simulation of delamination growth at CFRP-tungsten aerospace laminates using VCCT and CZM modelling techniques

The author performed the finite element analysis. The author and Kanerva wrote the manuscript.

# Original features

The following features are believed to be original in this thesis:

1. The applicability of the virtual crack closure technique (VCCT) in the case of yielding adhesive is demonstrated. It is shown that an elastic-plastic adhesive model can be used when the plastic deformation of the adhesive and energy release rate are numerically separated in the analysis. The error, caused by the usage of yielding adhesive in the VCCT analysis, is studied using the energy derivative technique (EDT). The error is shown to emerge at the beginning of crack growth, that is, during the crack onset phase. [P1]

2. Traditional analytical equations used in analyses of wedge peel tests neglect material nonlinearities. A two-dimensional VCCT analysis with linear material models was noted to result in similar initial crack lengths than the analytical equations. With yielding adherends, even a simple nonlinear material model applied for the adherends in the VCCT analysis was shown to provide a good correlation between the measured and calculated initial crack lengths. An increase in the wedge thickness (material yield) decreased the correlation. [P2]

3. A new analysis procedure separating the crack onset and propagation phases is developed. The method combines the VCCT and the cohesive zone model (CZM). The crack onset phase is modelled using the CZM and the crack propagation phase using the VCCT. The transition from the onset phase to the propagation phase is shown to be realistic and computationally converging. [P3]

4. The inability of the VCCT to analyse crack propagation in a hybrid cracked lap shear (CLS) specimen under residual stresses is revealed. The inability of the VCCT analysis is indicated by a significant crack propagation along the CLS specimen edges already under residual stresses. The unstable crack propagation also results in convergence problems when using an implicit finite element (FE) code. The CZM analysis was shown to provide a feasible crack propagation with respect to experiments when the stress criterion is fitted. The sensitivity of the CZM analysis to the stress criterion is, however, noticed. The developed combined VCCT-CZM method is shown to model the crack onset of

the CLS specimen even under residual stresses and mixed-mode crack-tip loading. [P4, P5]

# 1. Introduction

## 1.1 Background

Laminated composite structures and adhesively bonded joints are widely used in different applications, for example in aeronautical structures (Soutis, 2005; Higgins, 2000). The structures may get damaged during their lifetime (e.g. in the manufacturing process or due to impact loads) and they have to sustain such damage without the risk of catastrophic failure. Structures sustaining damage without losing their structural integrity are called *damage tolerant structures*. Alderliesten (2009) divides the current methods used in the design of damage tolerant structures into stress/strain methods and fracture-based methods.

Adhesively bonded joints and composite structures are typically designed by using stress/strain-based methodologies. Design methods for adhesive joints include analytical equations, such as those by Goland and Reissner (1944) and Hart-Smith (1973). The main advantage of analytical solutions lies in their simplicity. However, the solutions are typically only valid for relatively simple structures. Complicated geometries with sophisticated material models are nowadays designed using finite element (FE) analysis.

Especially when damage exists, damage tolerance has to be studied using fracture mechanics methods. Fracture mechanics is the study of the onset and propagation of cracks. The target of fracture analyses is to define the criticality of damage. Two fracture analysis methods are mainly used for interlaminar damage analyses. These are the virtual crack closure technique (VCCT) and the cohesive zone model (CZM) (Gustafsson & Waas, 2009).

The VCCT is originally based on Irwin's crack closure integral and it was further formulated for FE analyses. The VCCT evaluates the energy release rate (ERR) at the crack tip, based on local forces and displacements. The evaluation assumes that plasticity does not exist, that is, that the energy is fully consumed by the crack propagation. Another basic assumption of the method is that there is a pre-existing crack (Yang, 2005; Nguyen, 2013), meaning that the VCCT is not applicable for determining crack onset. The advantages of the method are its simplicity and robustness.

The applicability of the CZM modelling is broader when compared to the VCCT. The CZM allows modelling damage onset and propagation (Xie, 2006). Fracture analyses can thus be performed for structures without a pre-existing crack. The CZM modelling is based on a traction-separation law, which de-

scribes the damage onset and propagation. Various CZM laws have been introduced for delamination and debond analysis. A disadvantage of the method, when compared to the VCCT, is the higher number of parameters. The definition of traction-separation law parameters is typically based on fitting the analysis result with an experimental result, which does not allow the law to be unique. This is challenging in real-life applications where reference experiments cannot be performed.

## 1.2 Objectives and dissertation's structure

Fracture mechanics methods for delamination and debonding analyses have similarities, but the applicability of the methods differs in certain analysis cases. Naturally the performance of the applied method should be known to prevent mistakes that can lead to faulty decisions about structural integrity.

The objective of this thesis work is to study the limitations of the VCCT and CZM methods and to expand the applicability of the methods. Experimental results and results computed with established analytical equations provide the reference for the studies. The work consists of four different case studies, which are reported in detail in five scientific publications. The topics in the four case studies are:

- expanding VCCT analysis irrespective of adhesive yielding
- expanding VCCT analysis when accounting for adherend yielding
- forming a formulation for the crack onset
- the limitations of fracture models in hybrid laminates under mixed-mode loading and thermal stresses.

The objective of the first publication [P1] is to study the applicability of the VCCT method in the analysis of a bonded joint when the adhesive deforms plastically in the fracture process. Based on the related literature, the VCCT should not be applied in such a case. The structure being analysed in the study is a double cantilever beam (DCB) specimen.

The second paper [P2] continues the theme of studying the nonlinear material behaviour existing in the fracture process. In this study case, the adherend deforms plastically while the adhesive is presumed to have linear-elastic behaviour. The parameter being analysed is the precrack length of a wedge peel test specimen. The objective is to evaluate the error in the results provided by analytical equations and VCCT analysis.

The third publication [P3] has the objective of expanding the VCCT formulation to cover the crack onset. A new combined method of the CZM and the VCCT is developed for the purpose and is studied in detail in the crack onset and propagation analysis of a DCB specimen.

The objective of the last two publications [P4 and P5] was to study delamination damage in a hybrid laminate affected by rather inevitable thermal (cooling) loads and operation-related mechanical loads. The target was to find procedures for defining parameters for the crack onset and propagation in different modelling approaches. The applicability of both the VCCT and the CZM is covered. In addition, the applicability of the combined method described in

Publication 3 [P3] was studied in the analysis of crack onset under mixed-mode loading. The structure being analysed in the study was a cracked lap shear (CLS) specimen.

## 1.3 Limitations

The analysis studied in Publication 1 [P1] is limited to small-scale adhesive yielding. The linear-elastic and ideal-plastic models used in the study are simplified material models. This model simplifies material behaviour especially when plastic deformation begins. The limitation was seen to be acceptable because the plastic zone at the crack tip in the adhesive is relatively small and does not significantly affect the global response.

The study in Publication 2 [P2] was performed by assuming hypoelastic material behaviour for the adherends. This model does not involve permanent deformation, which would affect the results and the simulated crack growth when material was unloaded. This limitation was seen to be acceptable because unloading was expected to have a minor role in the precrack formation of a wedge peel test specimen. Linear elastic models were applied for other materials in the studies.

The studies in Publications 1 [P1], 2 [P2] and 3 [P3] were performed using a two-dimensional finite element analysis with plane strain elements. This approach neglects three-dimensional effects, such as two-dimensional crack growth.

The work in Publications 3 [P3] and 5 [P5] formulates a new method separating the crack onset and crack propagation. The method combines two different analysis methods. The work is primarily a feasibility study of this combined method. Only minor emphasis has been given to study sensitivity of the method to scalar fracture parameters and element type. This is clearly a topic that needs to be studied in future.

All numerical fracture analyses were performed using the implicit solution procedure (as implemented in Abaqus/Standard). The advantage of the implicit solution is its efficiency. The solution procedure affects the analysis when the damage is unstable and sudden, as in the fracture of the CLS specimen in Publications 4 and 5 [P4, P5]. In these cases, the implicit solution procedure suffered convergence problems. The use of the explicit solution procedure in these analyses is clearly an interesting topic for future studies.

# 2. Theoretical background

## 2.1 Elementary fracture mechanics

Materials include microscopic defects which may nucleate into macroscopic cracks. These cracks may propagate and lead to a catastrophic failure of the structures in which they appear. Knowledge about crack nucleation and propagation improves safety and the economics of structures when their load spectra are known. The field of research studying cracks in materials is called fracture mechanics, which is a branch of the field of mechanics.

Fracture mechanics is typically divided into linear-elastic fracture mechanics (LEFM) and elastic-plastic fracture mechanics (EPFM). LEFM is applied when the materials of a structure are brittle or when the plastic region of the structure is small compared to the structural dimensions. EPFM is applied when a significant part of the energy dissipates due to material plasticity.

Plastic deformation in LEFM typically refers to local plasticity at the crack tip, as illustrated in Figure 1. The local plasticity region is commonly described using the concept of the plastic zone radius. The plastic zone radius in an adhesively bonded joint can be evaluated using the equation

$$r_{\mathrm{p}} = \frac{1}{6\pi}\left(\frac{E_{\mathrm{a}} G_{\mathrm{C}}}{\sigma_{\mathrm{y}}^2}\right), \tag{1}$$

where $E_{\mathrm{a}}$ is the adhesive's Young's modulus, $G_{\mathrm{C}}$ is the fracture toughness and $\sigma_{\mathrm{y}}$ is the yield strength of the adhesive (ISO, 2009).

The plastic zone is caused by the stress peak at the crack tip. The crack tip is typically assumed to be sharp, which in a linear-elastic material leads to an infinite stress value at the tip. The stress decreases quickly when the distance to the tip increases (Figure 1).

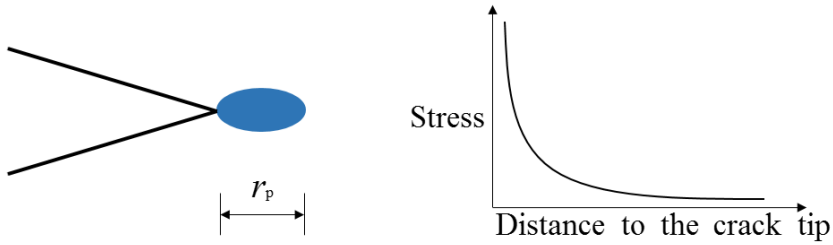


**Figure 1.** Plasticity (left) and stress distribution (right) at the crack tip.

The target of fracture mechanics is to understand the mechanisms of crack nucleation and propagation. Fracture mechanics is based on analyses and experiments. The analyses are commonly performed using an FE method or analytical equations. The aim of an analysis is to find a value for a parameter which describes the criticality of the applied load state when compared to the critical value provided by experiments. The applied parameter is typically either an energy or stress.

The applied energy parameter is based on the balance of the conserved energy, which can be presented as

$$\Delta W = \Delta U_e + \Delta W_p + \Delta W_s, \tag{2}$$

where $W$ is the work of the external force, $U_e$ is the elastic strain energy, $W_p$ is the plastic energy and $W_s$ is the energy release (Sun, 2002). The energy changes are assumed to be proportional to a new crack surface, $dA$. The assumption, with a rearrangement of terms, leads to the equation

$$R = \frac{dW}{dA} - \frac{dU_e}{dA} = \frac{dW_p}{dA} + \frac{dW_s}{dA}, \tag{3}$$

where $R$ is the fracture energy. The elements of the fracture energy are

$$G_p = \frac{dW_p}{dA} \text{ and } G = \frac{dW_s}{dA}, \tag{4}$$

where $G_p$ is the plastic dissipation and $G$ is the ERR.

Material fracture has been studied widely. The focus has mainly been on metals, which are typically ductile, dissipating part of the energy in the crack propagation process. Brittle materials and material systems do not have this feature. The ERR then mainly describes the fracture behaviour. Examples of brittle material systems are fibre-reinforced composite plastics. They are typically layered structures in which damage is typically delamination of the plies. Composite material systems have similarities with adhesively bonded joints, in which typical damage is debonding of the joint. Two fracture analysis methods, the VCCT and the CZM, are commonly used in debonding and delamination evaluations, as described in the following chapters.

## 2.2 Virtual Crack Closure Technique (VCCT)

The main development step in the VCCT's history is the work by Rybicki and Kanninen (1977). Irwin's crack closure integral formed a foundation for their work. Rybicki and Kanninen modified the integral into a form which can be implemented in the FE method. The crack tip in an FE model is characterised in Figure 2. The idea is to evaluate the ERR at the crack tip using the reaction force and separation between nodal points. Equations for defining the ERR in Mode I and II can be expressed in the form

$$\begin{aligned} G_{\mathrm{I}} &= \lim_{\Delta c \to 0} \frac{1}{2\Delta c} \bar{F}_{\mathrm{c}}(v_{\mathrm{c}} - v_{\mathrm{d}}), \\ G_{\mathrm{II}} &= \lim_{\Delta c \to 0} \frac{1}{2\Delta c} \bar{T}_{\mathrm{c}}(u_{\mathrm{c}} - u_{\mathrm{d}}), \end{aligned} \tag{5}$$

where $\bar{F}_{\mathrm{c}}$ and $\bar{T}_{\mathrm{c}}$ are the reaction forces, $u$ and $v$ are the displacements and sub-indexes refer to nodal points. Valvo (2012) stated that in some circumstances the VCCT's fracture mode partitioning can be physically inconsistent.

Equation (5) reveals the first assumption of the method, which is the linear relation between the reaction force and separation. Nonlinear mechanisms are thus not included in the model. Rybicki and Kanninen used a linear stiff spring between nodal points at the crack tip to provide a reaction force based on a predefined spring constant. Later, this approach was replaced by a two-step method in which the reaction force is first calculated at the crack tip. Secondly, crack-tip nodal points are detached and the separation is calculated. This procedure can also be performed vice versa because dissipation mechanisms do not exist.

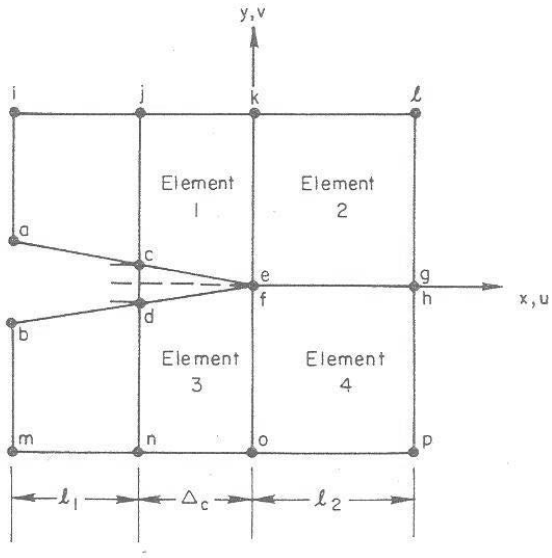


**Figure 2.** The crack-tip model (Rybicki, 1977).

The VCCT is also used by applying the so-called one-step method, in which the separation is computed in between the nodes adjacent to the crack tip (nodes c

and d in Fig. 2). This method includes an extra assumption which is that the stress state at the crack tip does not change remarkably (Bonhomme, 2009). The assumption is most often valid because the element length is typically small.

The basic equations of the VCCT are typically presented for two-dimensional plane strain or stress elements. However, the VCCT is widely used and the equations are available for many elements (Krueger, 2002). These include shell and solid elements. Equations for a singular element (Raju, 1986) and for kinking cracks (Xie, 2005a) have also been published.

Wang and Raju studied equations presented for shell elements (Wang, 1996). Their interest was to compare two possible formulations. In the first formulation, rotations and displacements were included for evaluating the ERR. In the second formulation, only displacements were taken into account. Based on the analysis, Wang and Raju concluded that the second formulation was feasible. This approach has been used since the results were published. The work also presented equations for taking into account element-width changes. Figure 3 presents the crack-tip model when using shell elements. The ERR equations for the shell elements are of the form

$$\begin{aligned} G_I &= -\frac{1}{2b\Delta a} Z_{Li}(w_{Ll} - w_{Ll^*}), \\ G_{II} &= -\frac{1}{2b\Delta a} X_{Li}(u_{Ll} - u_{Ll^*}), \\ G_{III} &= -\frac{1}{2b\Delta a} Y_{Li}(v_{Ll} - v_{Ll^*}), \end{aligned} \tag{6}$$

where $\Delta a$ is the element length; $b$ is the element width; $w, u, v$ are the displacements; and $X, Y, Z$ are the forces in the x, y and z coordinate axis directions respectively (Krueger, 2002). The formulation for solid elements is similar to the one for shell elements.

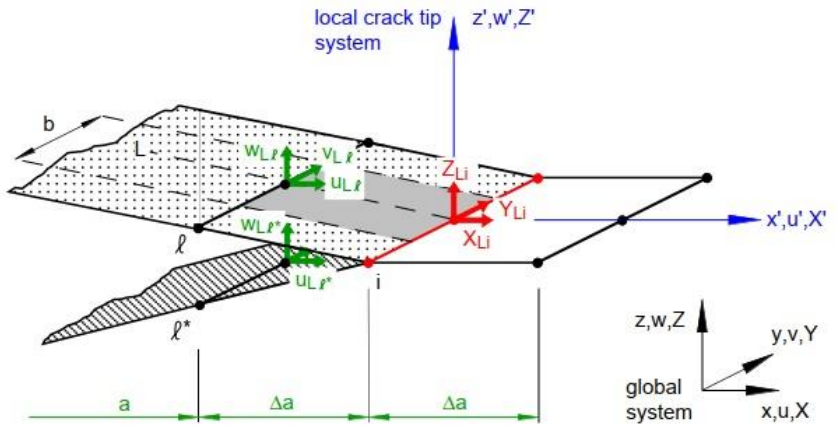


**Figure 3.** VCCT quantities at the crack tip when using shell elements (Krueger, 2002).

The VCCT has mainly been used in the delamination analyses of composites. The studied cases include, for example, embedded delaminations (Mikulik, 2008), skin-stiffener debonds (Krueger, 2009) and delaminations of face

sheets from sandwich cores (Goswami, 2001). Metal crack ERR evaluation has also been performed using the VCCT (Fawaz, 1998; Fawaz, 1999). In addition, the VCCT has been used to study delaminations in a leaching reactor made of glass fibre-reinforced plastic (Lindgren, 2016), debonding failures in a sandwich-composite cryogenic fuel tank (Glaessgen, 2005) and aircraft trailing-edge flap delaminations (Jokinen, 2015b).

The most simple delamination cases are standard fracture tests such as DCB experiments and end-notched flexure (ENF) experiments. Both experiments have been analysed using the VCCT in the literature (Meo, 2005; Tawk, 2010). The analyses have shown the applicability of the VCCT in cases where a constant fracture toughness and self-similar crack propagation are valid presumptions. The analyses of these experiments are also recommended for benchmark cases when validating FE codes (Orifici, 2012). The benchmarks are needed for validating results when numerical solution parameters also affect the result (Krueger, 2008; Pietropaoli, 2010).

Reported VCCT analyses of adhesively bonded joints are scarce. Yang et al. (2007) analysed a single lap joint with the VCCT to obtain a reference for a developed analytical method. Reference results for an analytical solution in a mixed-mode debonding case have also been calculated using the VCCT (Marannano, 2008). Xie et al. (2005b) studied the debonding of a steel hat stiffener. Kanerva et al. (2013) modelled microscale grooves at steel–epoxy interfaces.

The VCCT has further been used for analysing adhesively bonded DCB specimens in which the adherends were made of carbon fibre-reinforced plastic (CFRP) (Jiang, 2015) and CFRP/aluminium (Khoshravan, 2012). Xiao et al. (2009) used the VCCT in the case of an elastic-plastic (EP) material, stating that the VCCT can normally only be used with elastic materials. The results were compared with J-integral-based analysis results. The results indicated that the VCCT was applicable in the studied case of the plastically deformed, cracked specimen. Another VCCT application that included plastic deformation was the ERR calculation for shape memory alloys (Jape, 2016).

Another feature of the VCCT, in addition to the assumed linear elastic (or nearly linear elastic) material behaviour, is its requirement for a precrack. This requirement limits its use in crack onset simulations. Liu et al. (2010) stated that the VCCT is not competent for failure initiation analyses because the crack growth in a VCCT analysis should be self-similar. Self-similar growth means that the crack front remains similar when the crack propagates. However, the VCCT has also been used in analyses where fracture toughness is not constant (Shokrieh, 2012). A study of free-edge stresses is one application where the VCCT has been used for crack onset simulations. Free-edge stresses are caused by an elastic mismatch of layers in bi-material interfaces. Salpekar et al. (1996) studied free-edge delaminations using the VCCT with various delamination lengths. The comparison to an equivalent domain integral showed the VCCT to be a robust method for ERR calculation.

The VCCT has traditionally been used for evaluating the total ERR at bi-material interfaces (Agrawal, 2006). The speciality of the bi-material interface

is that Modes I and II ERR values are coupled (Sun, 1989) and mode-mixity can oscillate. The oscillatory part in the stress solution is typically analytically described using Dundur's parameters (Suo, 1990). The ERR components' non-convergence in a VCCT analysis is shown to be dependent on the element dimension (Raju, 1987). Beuth (1996) described a method based on the VCCT presenting a non-oscillatory solution dependent on the element dimension. Another solution for oscillation is to assume a resin-rich zone between materials (Raju, 1987). The oscillation is assumed to be negligible when the element dimension is close to the ply thickness (Krueger, 2002).

## 2.3 Cohesive zone model (CZM)

The CZM is based on the work of Dugdale (1960) and Barenblatt (1962). The Dugdale-Barenblatt crack model is presented in Figure 4. The basic idea of the model is to assume a 'cohesive zone' that exists ahead of the crack tip. The target of the approach is to avoid a stress singularity appearing at the sharp crack tip. Barenblatt's idea was to assume that the zone is affected by crack restraining cohesive stresses that are caused by atomic attractions. Dugdale assumed the crack tip to be longer in thin metal sheets because of yielding. (Rice, 1968)

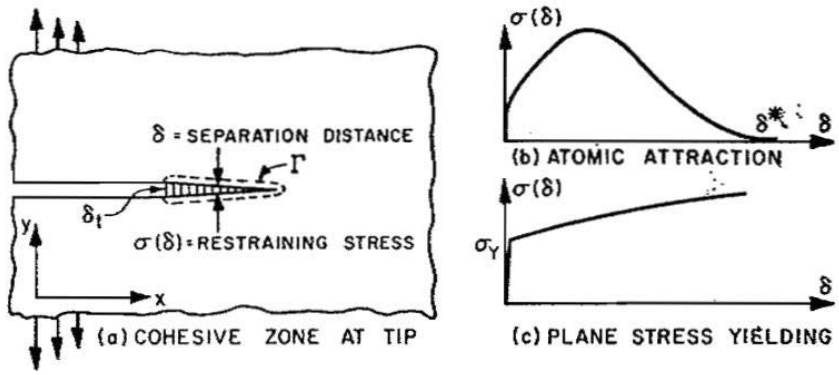


**Figure 4.** The Dugdale-Barenblatt crack model (Rice, 1968).

A cohesive zone model in an FE analysis is defined by using separate cohesive elements, which are attached to the studied interface. For that reason, the elements are also called *interface elements*. Xie et al. (2006) stated that interface elements divide into two types: continuous and discrete elements. Continuous elements are continuum elements. Discrete cohesive elements are typically spring elements. Lately, the cohesive surface approach, based on a contact pair, has been implemented in Abaqus (Abaqus, 2017a).

The deformation of cohesive elements in terms of stress (traction) and separation is defined using a constitutive equation, which is called the *traction-separation law*. Different types of laws are used. One of the simplest laws is the widely used bi-linear traction-separation law. Mathematically it can be expressed in the form

$$\sigma = \begin{cases} K\delta & \delta \leq a_0 \\ \frac{a_1-\delta}{a_1-a_0}\sigma_0, \text{ if } a_0 \leq \delta \leq a_1, \\ 0 & \delta \geq a_1 \end{cases} \quad (7)$$

where

$$a_0 = \frac{\sigma_0}{K} \text{ and } a_1 = \frac{2G_c}{\sigma_0}$$

(Alfano, 2006).

The initial part of the traction-separation law is typically linear. The stiffness of this initial part is described using the cohesive stiffness, $K$, which is defined before the analysis. Turon (2006) derived the cohesive stiffness from the one-dimensional Hooke's law. The derivation leads to an equation

$$K = \alpha E/t, \quad (8)$$

where $\alpha$ is the scaling factor, $E$ is the Young's modulus and $t$ is the thickness of the adjacent sub-laminate. Zou et al. (2002) derived the cohesive stiffness based on the strength of the interface material

$$K_{nn} = kZ_t, \quad (9)$$

where $Z_t$ is the interface strength and $k$ is the scaling factor. The scaling factor should be between $10^4$ and $10^7$ mm$^{-1}$ (Zou, 2002). Xie et al. (2006) stated that the cohesive stiffness should be at least a thousand times higher than the major Young's modulus of the body material. The interface becomes rigid when the cohesive stiffness increases. However, the utilisation of very high stiffness decreases analysis convergence (Turon, 2006).

The damage onset is defined by a fracture criterion, $f$. The fracture is assumed to occur when the criterion reaches the value of unity. The linear stress criterion for a single fracture mode can be characterised as

$$f = max\{\langle\sigma\rangle/\sigma_0\}, \quad (10)$$

where $\sigma_0$ is the critical stress.

Damage at the cohesive zone evolves and elastic properties start to degrade after the damage onset. The degradation area adjacent to the crack tip is described by the cohesive zone itself. The cohesive zone length can be estimated with the equation

$$l_{cz} = ME\frac{G_c}{\sigma_0^2}, \quad (11)$$

where $M$ is the parameter dependent on the cohesive zone model, $E$ is the Young's modulus, $G_c$ is the fracture toughness and $\sigma_0$ is the cohesive strength (Turon, 2006). The degradation is defined by the damage evolution law's formulation. The linear evolution of a bi-linear traction-separation law is an ex-

ample. Other damage evolution laws – such as linear-parabolic, exponential and trapezoidal laws – are shown in Figure 5. The most commonly used laws are the bi-linear law and the trapezoidal law (Campilho, 2013). A comprehensive list of damage evolution laws was presented by Shet and Chandra (2002). Appropriate parameter values for the laws can be defined comparing experimental and analysis results (Li, 2005). Xu et al. (2014) and Valoroso et al. (2013) have described inverse methods for defining the parameters.

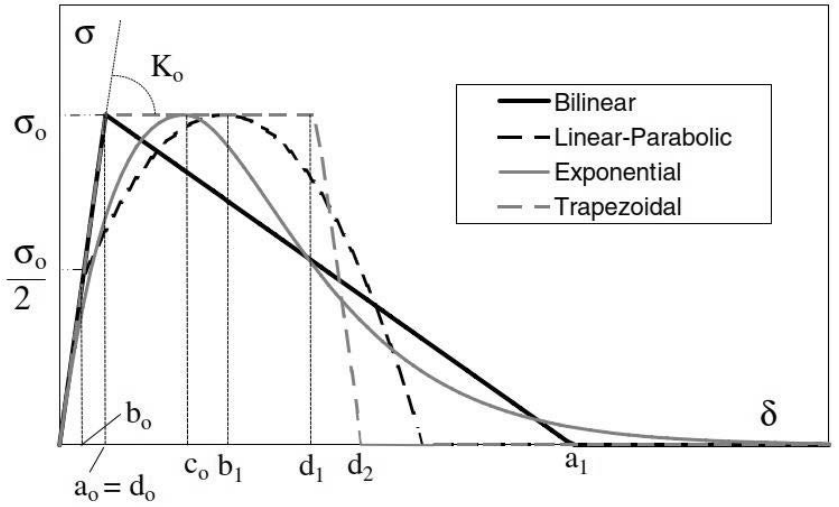


**Figure 5.** Different traction-separation laws (Alfano, 2006).

The applicability of laws has been discussed and sometimes the law's effect on results has been underrated in the scientific literature. Volokh (2004) showed that the applied law affected the results when studying a block-peel test. Campilho et al. (2013) stated that different laws can be used without compromising too much the accuracy of results when studying brittle adhesives. Freed and Banks-Sills (2008) and Alfano et al. (2009) have also studied the importance of the CZM law's shape. Alfano (2006) indicated that, in addition to the law's shape, a numerical perspective must be considered in analyses. A numerical perspective means, for example, the convergence of results. The cohesive strength is sometimes stated to be a parameter which does not have any effect on results. Typically, this parameter is numerically optimised.

The applications of the CZM modelling have a wide range, initiating from analyses of basic fracture specimens, such as the DCB and ENF specimens (Turon, 2007; Chen, 2010). Gustafsson and Waas (2009) studied how the parameters affect fracture specimen analysis results.

The CZM basically has two main benefits: the variety of damage models and the ability to model the damage onset without a pre-existing crack. The ability to modify the damage model allows the modelling of ductile adhesives (Campilho, 2008; Campilho, 2009). Various adhesive debonding analyses have been performed and reported (Feraren, 2004; Carvalho, 2017).

The CZM has been used for analysing the wedge peel test where adherend plasticity exists (Pardoen, 2005; Martiny, 2008; Ferracin, 2003). The CZM analysis was shown to be a feasible method in such cases. Pardoen et al. (2005) modelled constraint effects in the wedge peel test. The model is able to capture external and internal work. *Internal work* refers to the work in the cohesive elements, while *external work* includes the work (energy) stored in the adhesive and adherend. This allows taking into account both adherend and adhesive plasticity separately.

The CZM has also been used in analyses of bi-material interfaces (Anyfantis, 2014; Hirsch, 2017). Freed and Banks-Sills (2008) developed a new cohesive zone model for bi-material interfaces. However, the CZM is still relatively new in analyses of bi-material interfaces while the VCCT is an industrial standard (Goh, 2013). Guillamet et al. (2016) applied the CZM for modelling the free-edge delamination and compared the CZM analysis results with stress analysis results. The comparison indicated that the CZM relaxed singularities at the edge because of the cohesive zone. The CZM results were in good agreement when compared with the analytical solution proposed by O'Brien (1981).

The damage onset modelling capability of the CZM is an advantage in many applications. These include impact simulations (Camacho, 1996; Pärnänen, 2016), circular cut-out and edge delamination modelling (Goyal, 2004) and pipe delamination modelling (Zou, 2002). Xu and Needleman (1993) utilised the ability of crack onset modelling and the possibility to modify the damage model in a study of void nucleation.

# 3. Materials and methods

## 3.1 Adhesive plasticity

**The reference experiment and results**

DCB testing is a standardised method for defining fracture toughness, $G_{\mathrm{IC}}$, for an adhesive bond (ISO, 2009) and delamination (ISO, 2001). In the test, the crack is loaded under fracture mode I, as illustrated in Figure 6. The test includes two load cycles representing the crack onset and propagation. In the first, so-called insert cycle, a natural crack front is formed from the artefact front. In the second load cycle, called the precrack cycle, the crack is propagated. Fracture toughness, $G_{\mathrm{IC}}$, is computed using the force, $P$, the displacement, $\delta$, and the crack length, $a$. The computation is typically based on the corrected beam theory, which yields for the fracture toughness

$$G_{\mathrm{IC}} = \frac{3P\delta}{2B(a+|\Delta|)}\frac{F}{N}, \tag{12}$$

where $B$ is the specimen's width, $\Delta$ is the crack-length correction, $F$ is the large-displacement correction and $N$ is the load-block correction (ISO, 2009).

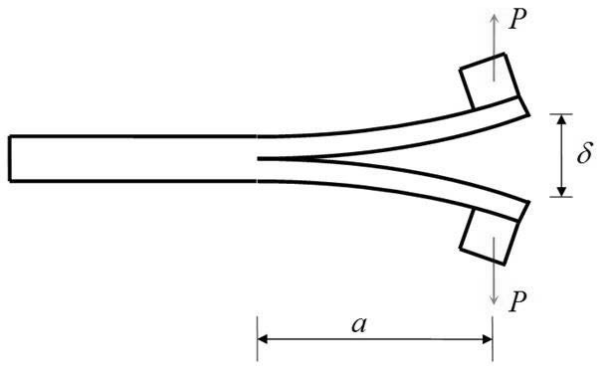


**Figure 6.** The DCB test [P1].

The reference DCB experiment for this thesis provided force-displacement curves for insert and precrack cycles (Figure 7). The fracture toughness values were determined from the test data using Eq. (12). Average $G_{\mathrm{IC}}$ values for the insert and precrack cycles were 1604 J/m² and 1820 J/m² respectively. The

coefficients of variation for the insert and precrack cycle $G_{IC}$ values were 7.3 % and 9.7 %, respectively.

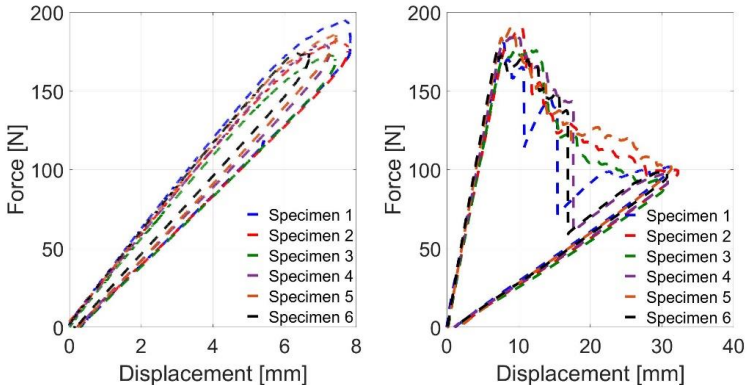


**Figure 7.** Experimental DCB force-displacement curves: the insert cycle (left) and precrack cycle (right) [P3].

## Materials

The DCB specimen consisted of an epoxy adhesive FM-300-2K (Cytec), aluminium Al7075-T76 adherends and loading blocks. Aluminium alloy Al7075-T76 was modelled using linear elastic properties. The applied Young's modulus was 71 GPa and the Poisson's ratio was 0.33 (MIL-HDBK-5J, 2003). The adhesive layer consisted of two FM-300-2K plies. The properties of the adhesive layer were estimated based on the work by Ishai et al. (1988). The adhesive was modelled using elastic and elastic-plastic properties. In both cases, the applied Young's modulus was 2.45 GPa and the Poisson's ratio was 0.38. The applied EP model was linear elastic and ideally plastic. The plasticity of the material model is based on a single parameter, the yield strength $\sigma_{ys}$. After reaching the yield strength, the stress-strain curve forms a plateau. The applied yield strength was 53 MPa. The applied EP material model is shown in Figure 8.

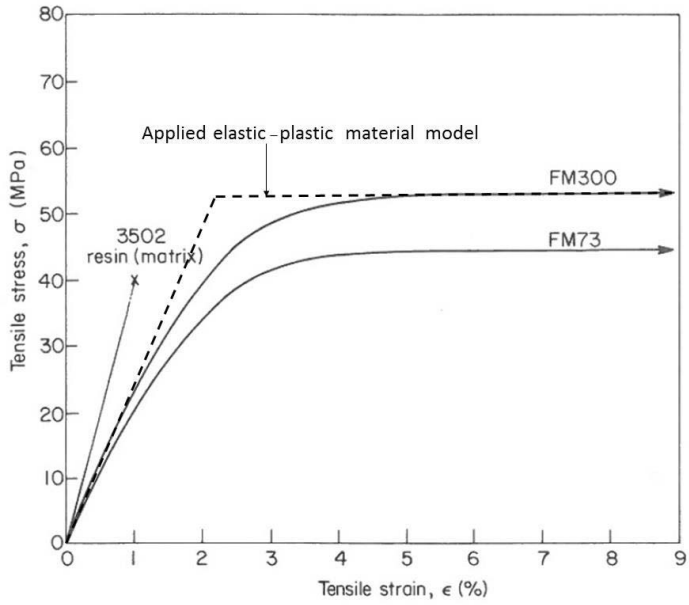


**Figure 8.** The applied linear elastic and ideally plastic material model of the adhesive [P1].

## Numerical analysis

The precrack cycle of the DCB test was analysed in Publication 1 [P1]. The VCCT analysis was initiated using linear elastic properties for the adhesive. The target was to compare the results of the linear analysis and experiments. The main target of the work [P1] was to study the applicability of the VCCT when the plasticity of the adhesive is accounted for in the analysis. The linear elastic and ideally plastic material model was thus applied for the adhesive in the second analysis phase. The experimentally measured average fracture toughness value was used in the linear analysis. The measured value takes into account the plastic deformation of the adhesive, meaning that it can be presented with the equation

$$R = G_{\mathrm{p}} + G, \tag{13}$$

where $G_{\mathrm{p}}$ is plastic deformation and $G$ is the ERR. Equation (13) indicates the equality of the fracture toughness and the ERR when plasticity is ignored. In the nonlinear analysis, the adhesive plasticity is taken into account by the material model and the plastic deformation should be separated from the critical ERR value used by the VCCT. The separation was performed iteratively to achieve similar crack propagation to that of the experiments. Finally, the study of different energy quantities on an FE basis was performed using the energy derivative technique (EDT). The EDT evaluates the energy values of reversible and permanent deformation using energy values and nodal failure data provided by the FE analysis. The energy derivative in the EDT was defined using a second-order Lagrange interpolating polynomial function (Fan, 2007).

The VCCT analysis was performed using a two-dimensional FE model (see Figure 9). The model was created using the commercial FE software Abaqus. The model included the adhesive plies, adherends and loading blocks. The tie constraint was defined between the adhesive and adherends, and between the loading blocks and adherends. The VCCT interface was defined between the adhesive plies. The adhesive was modelled using a plane strain element with incompatible modes (CPE4I). The adherends and loading blocks were meshed using a reduced integrated plane strain element (CPE4R).

The FE model boundary conditions were defined at the centre nodal points of loading blocks. In the lower point, both vertical and horizontal displacements were restricted. In the upper point, the horizontal displacement was restricted. The loading was performed using enforced displacement of the upper point. The enforced displacement followed the experimental average displacement. The unloading parts of both cycles were also modelled to determine permanent deformations similarly to experiments.

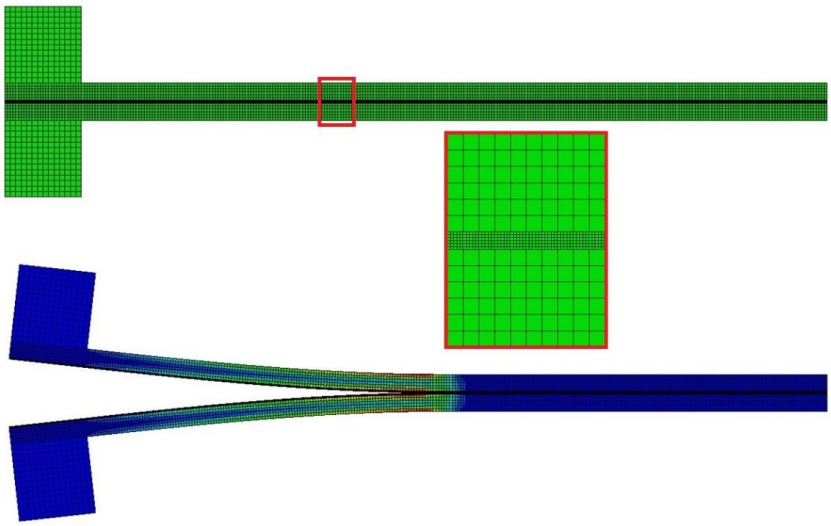

**Figure 9.** The applied FE model of the DCB specimen in undeformed and deformed shapes [P1]. The deformed shape related contour presents the von Mises stress distribution (red means high and blue low stress).

## 3.2 Adherend plasticity

### The reference experiment and results

The wedge peel test is used to determine the durability of an adhesive joint. In the test, a wedge is forced between the adherends, leading to a crack opening (see Figure 10). The initial crack length is measured after the enforcement. The specimen is then exposed to the desired environment and the crack length is measured after specified time intervals. The durability of the bond is defined by comparing measured crack lengths to pre-defined acceptance limits.

An analytical equation for estimating the fracture toughness in the wedge peel test is of the form

$$G_I = \frac{Y^2 E h^3 [3(a+0.6h)^2 + h^2]}{16[(a+0.6h)^3 + ah^2]^2}, \quad (14)$$

where $a$ is the crack length, $E$ is the Young's modulus of the adherend, $h$ is the adherend thickness and $Y$ is the thickness of the wedge (Stone, 1980). Plausinis and Spelt (1995) developed an improved equation, which takes into account the adhesive's effect on the test result. The equation takes the form

$$G_I = \frac{Y^2 E (h+h_a)^3 (1-h_a/(h+h_a))^3 (a+\beta)^2}{48(a^3/3 + a^2\beta + a\beta^2)^2}, \quad (15)$$

$$\beta = 0.667(h+h_a)\{(1-h_a/(h+h_a))^3(1+[h_a/(h+h_a)(2E/E_a-1)])\}^{1/4},$$

where $h_a$ is the thickness of the half-bond line and $E_a$ is the Young's modulus of the adhesive.

**Figure 10.** An illustration of the wedge peel test.

The only measured quantity in the wedge peel test is the crack length. The analysis work in this thesis focused on the initial crack length. Specimens with different adherend materials were prepared and tested. The measured average crack lengths of aluminium and titanium specimens are shown in Table 1. Corresponding test results of steel specimens (AISI304 and AISI4130N) are shown in Table 2. It should be noted that different wedge thicknesses were used in these tests to find an appropriate initial crack length for the steel specimens.

**Table 1.** Average initial crack lengths of aluminium and titanium wedge test specimens [P2].

| Adherend | Titanium Ti-6Al-4V | Aluminium 7075-T76 unclad | Aluminium 7075-T6 clad |
|---|---|---|---|
| Crack length [mm] | 42.7 | 42.9 | 38.8 |

**Table 2.** Average initial crack lengths of steel AISI304 and AISI4130N wedge test specimens with different wedge thicknesses [P2].

| Adherend / wedge thickness [mm] | Steel AISI304 | Steel AISI4130N |
|---|---|---|
| 3.2 | 31.5 | 38.4 |
| 4.2 | - | 41.5 |
| 4.9 | 35.7 | 49.0 |
| 6.0 | 38.6 | - |

## Materials

The same epoxy adhesive ply (FM-300-2K) was used for wedge test specimens as that used in Publication 1 [P1] but the number of adhesive plies was different (one instead of two [P2]). The adhesive ply included a knit carrier, which has an influence on the adhesive fracture. The fracture toughness for the adhesive was defined based on the earlier test results of 171 wedge peel specimens in total [P2]. The fracture toughness was computed from the measured initial crack lengths using Eq. (15). The average fracture toughness was 1,324 J/m² and the specimens had a standard deviation of 8.4 per cent in the initial crack length.

In all the VCCT analyses of wedge test specimens, the adhesive was modelled as being linear elastic. The applied adhesive properties were $E$ = 2.45 GPa and $\nu$ = 0.38 (Ishai, 1988). Titanium (Ti-6Al-4V), unclad aluminium (7075-T76) and clad aluminium (7075-T6) adherends did not yield in the tests and they were modelled as linear elastic materials. The applied titanium and aluminium Young's moduli were 110 GPa and 71 GPa respectively (MIL-HDBK-5J, 2003). A Poisson's ratio of 0.33 was used for all metal adherends in the study.

The deformation plasticity material model of Abaqus was used for the steel (AISI 4130N and AISI304) adherends that yielded in some test series. The model is a nonlinear elastic model because permanent deformation is not included (Abaqus, 2017b). The deformation plasticity model takes the form

$$E\varepsilon = \sigma + \alpha(|\sigma|/\sigma^0)^{n-1}\sigma, \tag{16}$$

where $\alpha$ is the yield offset, $n$ is the hardening exponent and $\sigma^0$ is the yield stress (Abaqus, 2014). The applied deformation plasticity model parameters were computed from tensile test results of the materials. The test results and the applied material models for the steels are shown in Figure 11 and 12. The parameter values are listed in Table 3.

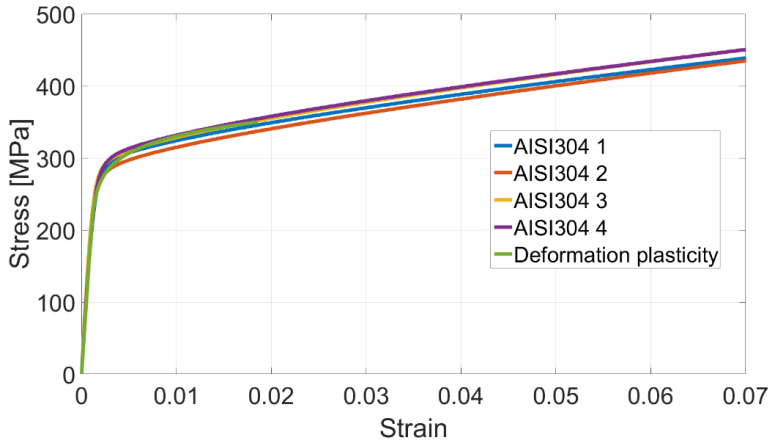


**Figure 11.** The measured AISI304 stress-strain curves and the applied deformation plasticity model [P2].

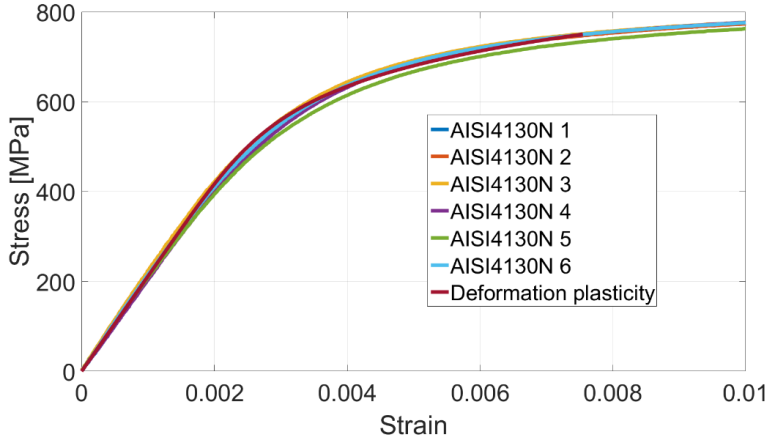


**Figure 12.** The measured AISI4130N stress-strain curves and the applied deformation plasticity model [P2].

**Table 3.** The applied material parameters of the deformation plasticity model for AISI304 and AISI4130N [P2].

| Material | $E$ [GPa] | $\alpha$ | $n$ | $\sigma^0$ [MPa] |
|---|---|---|---|---|
| AISI304 | 197.4 | 1.74 | 12.00 | 300.0 |
| AISI4130N | 211.7 | 0.06 | 8.24 | 500.0 |

## Numerical analyses

The initial crack lengths of wedge peel tests were analysed using analytical methods (Eq. (14) and (15)) and the VCCT. The results were further compared with the experimental data. The VCCT analyses were performed with a two-dimensional FE model. The deformed model is shown in Figure 13. The specimen included the adherends and the adhesive, bonded together using the tie constraint. In addition to the specimen, the wedge was modelled. The contact was defined between the wedge and the adherends. The model was meshed using a two-dimensional plane strain element for the specimen (CPE4I) and for the wedge (CPE4R). Boundary conditions were defined at the wedge end. A horizontal displacement of 25 millimetre forced the wedge into the specimen while opening the crack. The vertical displacement was restricted at the wedge end. At the opposite end of the specimen, displacements in vertical and horizontal directions were restricted. The model geometry was set to correspond to the experimental specimen being analysed.

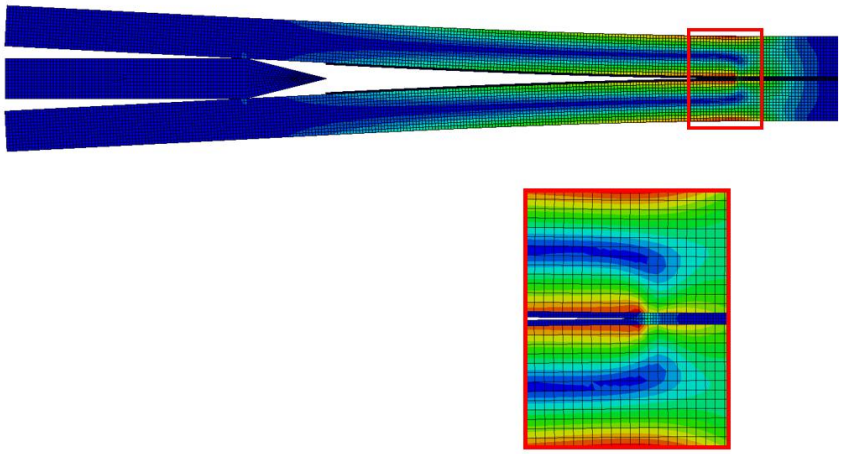

**Figure 13.** The wedge test specimen's FE model in a deformed shape [P2]. The contour presents the von Mises stress distribution at the deformed shape (red means high and blue low stress).

## 3.3 Crack onset

### Reference experiments and results

The reference experiment in Publication 3 [P3] was the DCB test described in Section 3.1. The reference was mainly the insert cycle because the focus was on the crack onset. The DCB tests provided reference force-displacement curves (Fig. 7) and the average fracture toughness value for analyses.

In addition to the DCB test, the out-of-plane strength of the adhesive, provided by a butt joint (BJ) test, was used in the analyses of this thesis. The BJ test is a standardised test method for defining the adhesive out-of-plane strength (ISO, 1987). The BJ specimen consisted of aluminium (6062) adherends bonded with the epoxy adhesive FM-300-2K. The cylindrical cross-section specimen was loaded by tensile loading as shown in Figure 14. The measured average out-of-plane strength based on the maximum force and the cross-sectional area was 27.35 MPa ± 1.52 MPa.

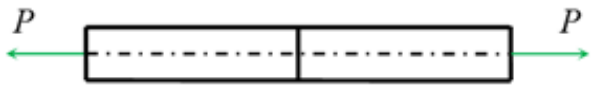


**Figure 14.** The BJ specimen and loading.

### The materials and numerical analyses

A combined method of the VCCT and the CZM was developed in Publication 3 [P3]. In this method, the CZM is used to provide the crack onset and the VCCT is used to analyse the crack propagation phase. The method is introduced in Figure 15. It allows the analysis of the nucleation and self-similar propagation phases with different material parameters. The method combines the benefits of the CZM and the VCCT into a single analysis.

The approach for defining the combined method for the reference DCB test is described in Figure 16. The DCB test provided fracture toughness values for the crack onset and propagation phases. The transition point is defined based on the average crack propagation during the insert cycle. The transition point was set to 3.9 mm adjacent to the original crack tip. The nucleation parameter, cohesive strength, is fitted based on the force-displacement curve of the insert cycle (Jokinen, 2017). The transition point and cohesive strength, in addition to fracture toughness values, provide sufficient parameters for performing the combined CZM-VCCT analysis.

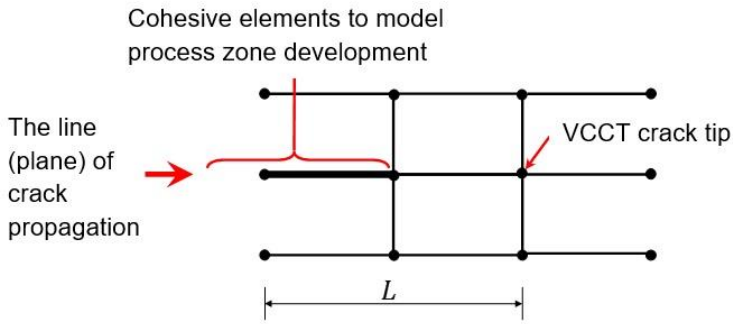


**Figure 15.** Characterisation of the combined CZM-VCCT method [P3].

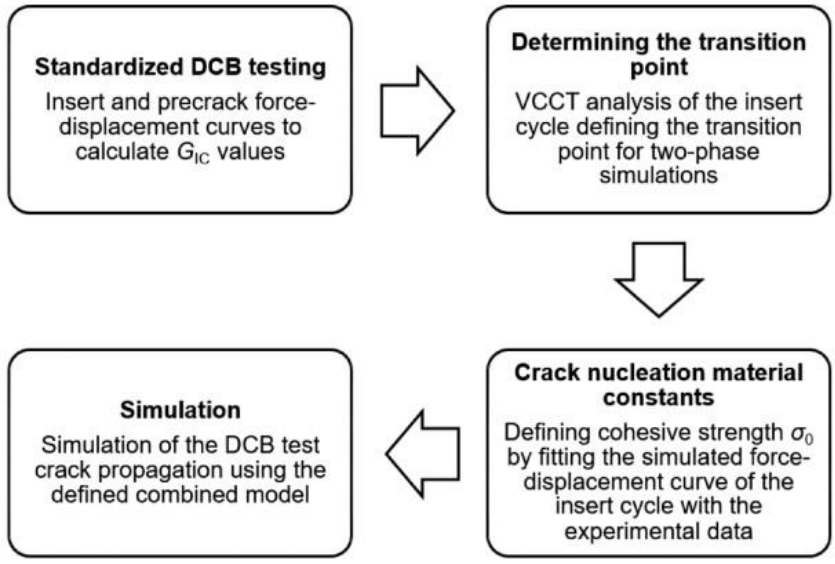


**Figure 16.** The approach defining the combined CZM-VCCT model for DCB analysis [P3].

In Publication 3 [P3], the DCB specimen's FE model was based on the model described in Section 3.1. The model was modified for the combined method and CZM analyses. In these analyses, CZM elements (COH2D4) were added to the interface. In addition to the combined CZM-VCCT model, three models

were created for comparison. All four models are shown in Table 4. In the single-phase CZM model, the measured BJ strength was used as a cohesive strength value and the applied fracture toughness value was same in the nucleation and propagation models. In the two-phase CZM model, the applied parameter values were equal with the values used in the combined CZM-VCCT model. The usage of two different parameter sets in the two-phase CZM analysis leads to different cohesive zone lengths in the nucleation and propagation phases. The two-phase VCCT model was based on fracture toughness values measured for the insert and precrack cycles in the DCB tests. The last column of Table 4 presents the transition zone length applied to two-phase methods. The element length in the combined and two-phase CZM models was 0.1 mm, which provided 38 elements for the transition zone.

**Table 4.** The applied FE models of the DCB specimen [P3]. The fracture toughness values and the cohesive strength values (when needed) applied in nucleation and propagation models.

| Method | Nucleation model, parameters | Propagation model, parameters | Transition zone length (mm / number of CZM elements) |
|---|---|---|---|
| CZM (single phase) | CZM: 1820 J/m², 27.35 MPa | CZM: 1820 J/m², 27.35 MPa | -/- |
| VCCT (two phase) | VCCT: 1604 J/m² | VCCT: 1820 J/m² | 3.9/0 |
| Combined (two phase) | CZM: 1604 J/m², 150 MPa | VCCT: 1820 J/m² | 3.9/38 |
| CZM (two phase) | CZM: 1604 J/m², 150 MPa | CZM: 1820 J/m², 27.35 MPa | 3.9/38 |

## 3.4 Hybrid laminate

### The reference experiment and results

The reference experimental configuration for Publications 4 and 5 [P4, P5] was the CLS specimen (Fig. 17), which is a typical mixed-mode (mode I and II) fracture specimen. The specimen includes an initial crack at the end of the lap. The length of the lap is not equal to the strap length, which causes asymmetry and a bending moment at the crack tip.

The well-known analytical equation of the CLS specimen provides the total ERR at the crack tip. The equation for the ERR can be extracted in the form

$$G = \frac{1}{2E_s^*}\left(\frac{F^2}{h_s} + 12\frac{M_1^2(l_A)}{h_1^2}\right) + \frac{1}{2E_l^*}\left(-\frac{F^2}{Ah_s} - \frac{M_0^2(0)}{Ih_1^2}\right), \quad (17)$$

where $F$ and $M$ are force and moment, $A$ and $I$ are coefficients, sub-indexes $l$ and $s$ refer to the lap and strap, and 0 and 1 refer to the bonded and unbonded sections respectively. The mode-mixity $\psi = \tan^{-1}(K_{\mathrm{II}}/K_{\mathrm{I}})$ can be derived following the procedure of Lai et al. (1996). The analytical method as a specific

solution in Publication 4 [P4] is described in the appendix of that publication [P4]. A semi-empirical method using strain gauges (attached to the CLS) has also been developed (Wilkins, 1981; Grady, 1992). The CLS specimen was equipped with strain gauges, as shown in Figure 17. In addition to strains, the loading (force) was recorded in tests. The measured average failure force was 11.8 kN (Kanerva, 2015a).

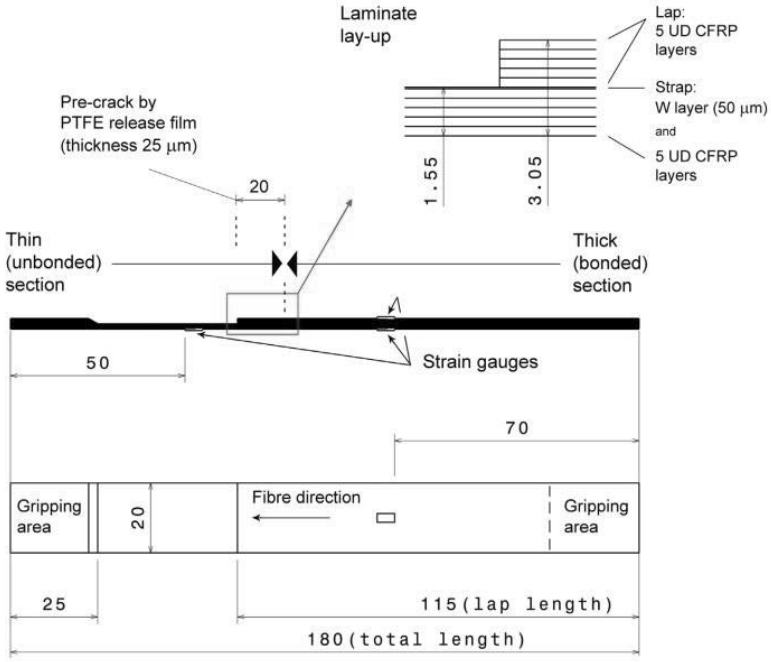


**Figure 17.** The CLS specimen [P4].

## Materials

The CLS specimen laminate included 10 unidirectional CFRP plies and one tungsten (W) ply. The tungsten ply was a mechanically rolled foil with a purity of 99.95 % (Alfa Aesar GmbH, Germany) and the CFRP plies were of a pre-preg tape (Advanced Composites Group, Umeco, UK), which consisted of MTM® 57 epoxy resin (ACG, UK) and unidirectional high-modulus M40J(12K) carbon fibres (Toray, USA) (Kanerva, 2015a). The stacking sequence of the specimen was $[(0)_5/W/(0)_5]$. The adhesion between the CFRP and tungsten plies was based on the pre-preg epoxy resin, i.e. no adhesive plies were used. The crack was located at the interface of the tungsten and the CFRP ply, and the tungsten ply was continuous in the strap. CFRP and tungsten were modelled as being linear elastic using the material properties shown in Table 5. The stiffness of the tungsten ply is much higher than the stiffness of the CFRP. The stiffness difference results in residual stresses when the specimen is cooled down from a stress-free temperature to the ambient temperature. The temperature change due to the cure cycle was 100 °C.

**Table 5.** The applied material properties of the CLS specimen [P4].

| | CFRP | Tungsten |
|---|---|---|
| $E_{xx}$ [GPa] | 191.5 | 410 |
| $E_{yy}$, $E_{zz}$ [GPa] | 6.3 | 410 |
| $E_{xy}$, $E_{yz}$, $E_{xz}$ [GPa] | 7.2 | (160.2) |
| $\nu_{xy}$, $\nu_{yz}$, $\nu_{xz}$ [-] | 0.31 | 0.28 |
| $CTE_{xx}$ [$10^{-6}$ 1/°C] | -0.43 | 4.5 |
| $CTE_{yy}$, $CTE_{zz}$ [$10^{-6}$ 1/°C] | 44 | 4.5 |

## Numerical analysis

The measured average failure force was used to compute the critical ERR value for further use. The critical ERR value was computed with the analytical equation Eq. (17) and with a three-dimensional VCCT model that included both temperature change and tensile loading. The crack propagation was studied using the VCCT, the CZM and the combined CZM-VCCT method. The experimental force-strain curves were compared with the numerical results for method validation purposes. The CZM parameters were iterated based on the curve comparison. The combined CZM-VCCT method used the same material properties as the fitted CZM model.

The FE model was three-dimensional, as shown in Figure 18. The model had an interface between the lap and strap (Figure 17). Each of the fracture models was attached to this interface. Separate CZM elements were defined for CZM and combined CZM-VCCT analyses. In the combined model, the VCCT zone was surrounded by the crack nucleation zone at the crack tip and at the edges of the CLS specimen. One CZM element (in depth) was used to model the nucleation zone. The VCCT and the CZM models were analysed with and without a temperature step describing the cure cycle (in Abaqus). In the tensile load step, displacement boundary conditions were set at both ends of the specimen. The displacements were restricted, excluding the longitudinal enforced displacement that was defined for the tensile load step.

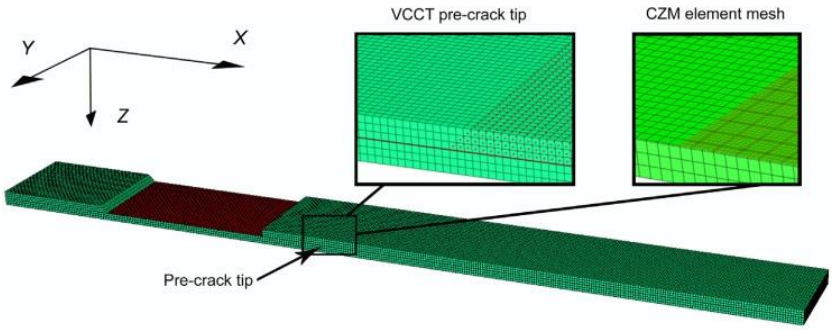


**Figure 18.** The FE model of the CLS specimen [P4].

# 4. Results and discussion

## 4.1 Adhesive plasticity

The VCCT is commonly applied in composite laminate delamination analyses. Adhesive debonding is a similar interlaminar failure, but typically more ductile than delamination. The target of Publication 1 [P1] was to study the applicability of the VCCT debonding analysis when the adhesive behaves elastic-plastically. The precrack cycle of the DCB test, as described in Section 3.1, was selected for the analysis case.

The study was initiated by comparing linear VCCT analysis results with experimental results. This also characterized the applied model for the case. Next, adhesive yielding was taken into account by applying an EP material model for the material. The applicability of the VCCT was concluded by conducting an EDT analysis.

The experimental average fracture toughness, computed with Eq. (11), was used in the linear analysis. Figure 19 provides a comparison of linear VCCT analysis results and three experimental force-displacement curves (specimens A2, A3 & A5). The comparison shows that the analysis results matched well with the experimental data. The results differed slightly at the maximum force where the analysis did not provide similar nonlinearity to the experiments. The crack onset occurred at the maximum force. The correlation between experimental and analysis results after the maximum force region indicates the usability of the constant fracture toughness in the reference case. The constant fracture toughness refers to the existence of a self-similar crack growth where the crack tip remains constant after it has formed.

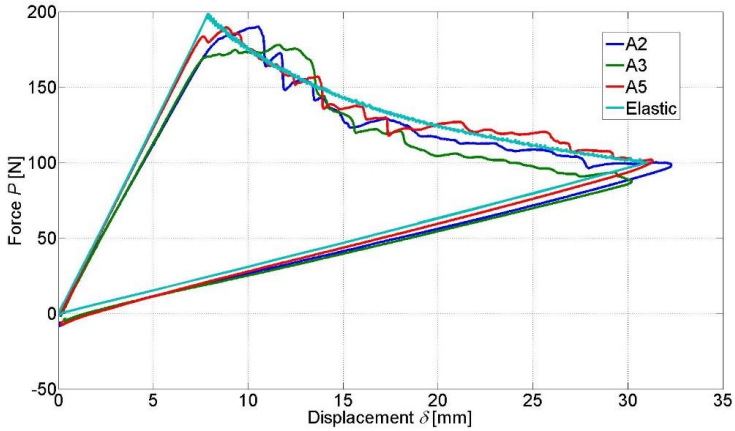


**Figure 19.** Three experimental DCB force-displacement curves (A2, A3 & A5) of the precrack cycle and the linear VCCT analysis results of the cycle [P1].

The fracture toughness value used in the linear analysis included the energies required for crack formation (ERR $G$) and for plastic dissipation ($G_{\mathrm{p}}$). When an EP material model is applied for the adhesive, these energies must be separated since an appropriate $G_{\mathrm{IC}}$ value in this analysis case is ERR $G$. The separation was performed iteratively by conducting EP VCCT analyses with different $G_{\mathrm{IC}}$ values to obtain a good match with the linear analysis force-displacement curve.

The comparison of elastic and EP analysis force-displacement curves is shown in Figure 20. It can be seen that the EP analysis with the value $G_{\mathrm{IC}}$ = 1275 J/m² provides a similar force-displacement curve to the linear analysis (and the experiments). The small difference between these two curves lies mainly at the maximum force. The EP analysis did not significantly improve match with the experimental curve at the crack onset when compared to the linear analysis. The EP analysis also faced numerical difficulties in this area.

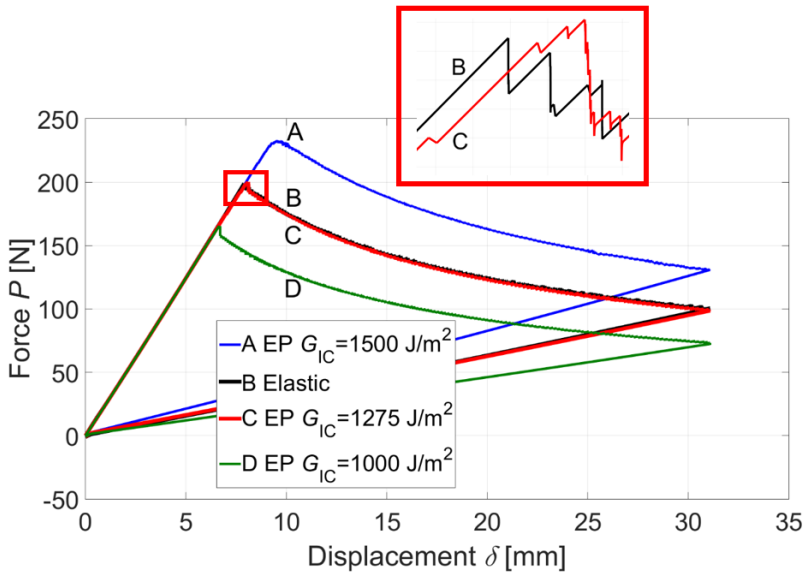


**Figure 20.** The force-displacement curves of the DCB precrack cycle obtained with an EP VCCT analysis using different $G_{IC}$ values (the result of an elastic analysis is shown as a reference) [P1].

The EP analysis ($G_{IC}$ = 1275 J/m²) was studied in more detail using the EDT, which defines energy quantities based on energy values and the fracture area. The applied FE software, Abaqus, provided the energy values (such as plastic energy and elastic strain energies). The fracture area was calculated from nodal releases of the analysis. The EDT analysis results are shown in Figure 21. It can be seen that the fracture toughness $R$ of the EP analysis is at the level of 1800 J/m², which is similar to the experiments. This is understandable because the $G_{IC}$ value applied in the EP analysis was iterated in order to obtain a good match with the experimental force-displacement curve. The distinction between the fracture toughness and the elastic $G$ is plastic dissipation because other dissipation mechanisms do not exist in the analysis.

The main result of Figure 21 is seen when comparing the ERR $G$ values used in the VCCT analysis and EDT $G$ values computed at the beginning of crack propagation. The EDT values are seen to be smaller than the VCCT values but reach the same level when the crack propagates. The small oscillation in the VCCT value is due to the applied tolerance of the critical $G$ value, which was used to improve convergence (in Abaqus).

Effects of the applied tolerance have not been studied widely in literature (Pietropaoli, 2010) but is has been reported that unsatisfactory results may also be achieved (Krueger, 2008). In the current case the tolerance can delay the crack onset when the critical ERR value is allowed to be exceeded and have an effect on the number of analysis increments (Jokinen, 2015a). The effect of the tolerance is naturally case dependent.

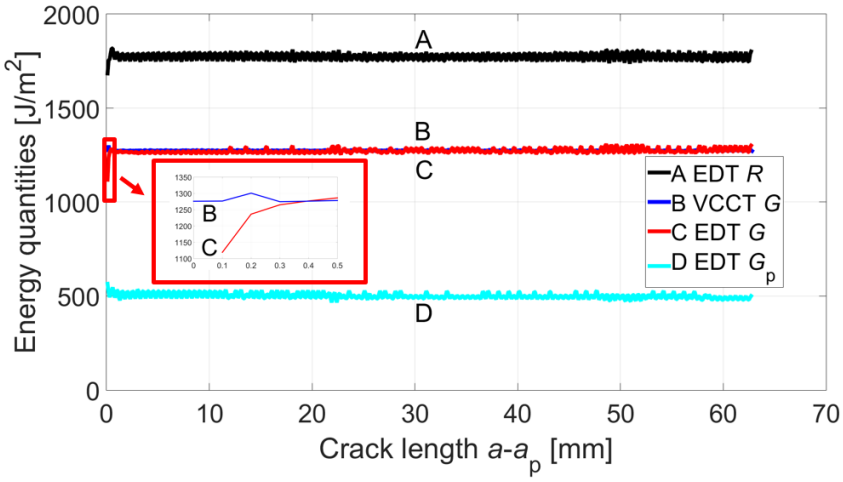


**Figure 21.** EDT analysis results and critical values used by the VCCT in Abaqus [P1].

The achieved EP result demonstrates the ability of VCCT analysis to perform simulations even when adhesive plasticity exists in the model. Fan et al. (2007) stated that the VCCT cannot be used in the case of nonlinear elasticity or plasticity. Xiao et al. (2009) stated that the VCCT typically underestimates fracture energy. The EP analysis results show that total prohibition of the VCCT analysis is too restrictive. This conclusion is limited to small-scale yielding since adhesive plasticity with respect to the global response of the DCB specimen was relatively small.

The main error in the VCCT analysis occurs at the crack onset. The magnitude of the error is less than 15 percent in the value of $G$. The momentary error decreases rapidly along with the crack propagation. The influence of the error on analysis results is thus relatively small. The explanation for the error lies with the VCCT practice of computing the reaction force and separation at different nodal points, based on the assumption that the stress state does not change remarkably between adjacent nodal points (Bonhomme, 2009). This assumption is not realistic at the crack onset of the yielding adhesive due to different yield states of the nodal points. When the crack propagates, the difference diminishes and adjacent nodal points are in a similar strain state. This is illustrated in Figure 22, where the colour distribution presents plastic strain when the crack has propagated almost one millimetre (precrack cycle, force $P$ = 200 N). Figure 22 also presents the reaction force $F_i$ and separation $\delta u_i$ used by the VCCT (the sub-index refers to $i^{\text{th}}$ nodal failure order number). At the first nodal failure, a small plastic strain exists in the reaction force nodal point while the plasticity is negligible in the separation nodal point. When the analysis proceeds, the loading decreases the difference of strain states between the reaction force and separation nodal points. At the fourth nodal failure, plastic strains are already close to each other. The reaction force and separation nodal points are practically in a similar strain state when the crack has propagated over nine elements (i.e. less than a millimetre).

Self-similar crack growth is attained in the studied case shortly after the crack onset. This agrees well with the plastic zone size evaluated using Eq. (1). The equation provides a plastic zone radius of 0.19 mm when the applied analysis parameter values (2.45 GPa, 1820 J/m² and 53 MPa) are used. In general, the error of the process is dependent on the material model and FE mesh. The finer the element size, the better the fulfilment of the VCCT's assumption.

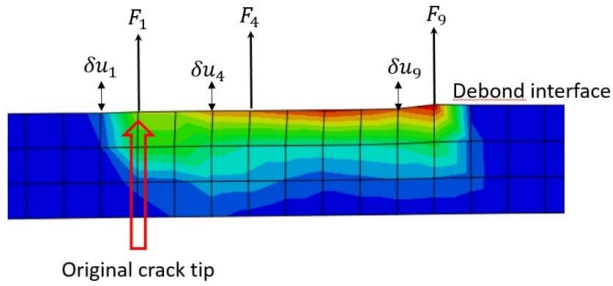


**Figure 22.** The evaluation of reaction forces and separation when the crack has propagated (precrack cycle, force $P$ = 200 N). The colour distribution demarks plastic strain (colours from blue to red refer to a plastic strain level ranging from negligible to high).

## 4.2 Adherend plasticity

Publication 2 [P2] continued the study of using a nonlinear material model in the VCCT analysis. The publication focused on the evaluation of an initial crack length in the wedge peel test. Reference experiments included aluminium, titanium and steel adherends with the same adhesive. Aluminium and titanium adherends remained elastic in the experiments. The steel adherends yielded, and they were modelled using a nonlinear material model. The applicability of VCCT analyses was evaluated by comparing experimental and computed initial crack lengths.

The analyses were initiated by studying aluminium and titanium specimens. Table 6 presents a comparison of experimental results and initial crack lengths computed with Eq. (15). It can be seen that, in general, Eq. (15) provides shorter crack lengths when compared to the measured average crack lengths.

Table 6 further provides a comparison of computed initial crack lengths. The results indicate that Eq. (14) provides a few percent longer crack lengths than Eq. (15), which takes into account the adhesive while Eq. (14) does not. Presumably, this is explained by the stiffer behaviour of the specimen when the adhesive is included. A linear VCCT analysis provides a few percent shorter crack lengths than those from Eq. (15). The applied tolerance may have a minor influence on VCCT results. In general, all analysis results are close to the measured average crack length values, especially when taking into account the standard deviation that existed in the experiments, defining the fracture toughness.

**Table 6.** Aluminium and titanium wedge peel test and analysis results.

| Material | Initial crack length comparison [%] | | |
|---|---|---|---|
| | Test vs. Eq. (15) | Eq. (15) vs. Eq. (14) | Eq. (15) vs. VCCT |
| Al. 7075-T76 unclad | -7.06 | 2.36 | -2.61 |
| Al. 7075-T6 clad | 2.76 | 2.36 | -2.61 |
| Ti-6Al-4V | -7.87 | 2.50 | -0.53 |

Table 7 shows the corresponding results for steel (AISI4130N and AISI304) specimens with different wedge thicknesses. Crack lengths computed for AISI4130N specimens with Eq. (15) are close to the measured values. A good correlation of the results verifies that the adherend plasticity in these specimens was relatively low. As for aluminium and titanium specimens (see Table 6), the VCCT provides shorter crack lengths and Eq. (14) provides longer crack lengths than Eq. (15).

The adherends of AISI304 specimens yielded when the wedge was forced between the adherends. Consequently, initial crack lengths provided by Eq. (15) are 15.5 to 31.3 percent higher than the measured average crack lengths. The increase of wedge thickness increased the difference. Crack lengths provided by Eq. (14) are again higher than those provided by Eq. (15).

The applied deformation plasticity model improved the correlation between VCCT analysis results and AISI304 experimental data. The hypoelastic material model decreased the specimen stiffness by taking into account material nonlinearity, which decreased the crack growth. With the lowest wedge thickness, the VCCT-simulated crack length is very close to the measured average crack length. According to Table 6, the difference between the VCCT's and Eq. (15)'s analysis results is almost constant with all wedge thicknesses, meaning that VCCT analysis performs best with the lowest wedge thickness. Lower performance with higher wedge thicknesses is at least partly explained by the fact that permanent deformation and plastic dissipation of the specimen are not taken into account in the applied fracture toughness value of the adhesive.

**Table 7.** Steel AISI4130N and AISI304 wedge peel test and analysis results.

| Material | $Y$ [mm] | Initial crack length comparison [%] | | |
|---|---|---|---|---|
| | | Test vs. Eq. (15) | Eq. (15) vs. Eq. (14) | Eq. (15) vs. VCCT |
| AISI4130N | 3.2 | -3.77 | 3.60 | -2.51 |
| AISI4130N | 4.2 | 3.01 | 3.12 | -1.26 |
| AISI4130N | 4.9 | -5.35 | 2.89 | -1.32 |
| AISI304 | 3.2 | 15.50 | 3.55 | -14.83 |
| AISI304 | 4.9 | 27.65 | 2.85 | -13.80 |
| AISI304 | 6.0 | 31.32 | 2.59 | -13.33 |

The adhesive fracture when adherends deform plastically has been modelled successfully using the CZM approach (Ferracin, 2003; Yang, 1999). Hadavinia et al. (2006) showed fracture toughness $G_C$ to be independent of geometric

parameters of the specimen and to describe interface properties when CZM is used. However, the performance of the applied VCCT analysis technique was dependent on the wedge thickness. The VCCT provided a better prediction of the initial crack length when compared to analytical equations, and a perfect match was not achieved.

## 4.3 Crack onset

The VCCT has been shown to be beneficial in crack propagation analyses. The method does not require extra material parameters in addition to standard fracture toughness (along with the fracture criterion). It also assumes a linear relation of parameters applied in the definition of ERR. The limitation of the VCCT is the requirement of a pre-existing crack, which limits its use to cases with existing damage. The CZM is able to provide the crack onset but at the expense of extra (material) parameters. It also allows the usage of different traction-separation laws.

A new method separating the crack nucleation and propagation phases was developed in Publication 3 [P3]. In the method, the nucleation phase is modelled using the CZM and the propagation phase is modelled using the VCCT. In Publication 3 [P3], the combined CZM-VCCT method was used for the simulation of DCB experiments [P1], which include two load cycles representing two different fracture phases with different physics. The results provided by the new method were compared to the results provided by pure VCCT and CZM analyses.

**Crack onset**

The numerical and experimental results of the DCB test related to the crack nucleation phase (the so-called insert cycle, initiated from the insert film [ISO, 2009]) are shown in Figure 23. Material parameters applied in numerical analyses are given in Section 3.3. The combined method is seen to provide a similar shaped force-displacement curve to that of the experiments while the stiffness of the model (the slope of the initial curve) is higher. In contrast to the combined method, the single-phase CZM model produces a relatively flat curve, meaning that the stiffness degradation of CZM elements occurs at a low force level. The dissipation energy, given by the enclosed area defined by the force-displacement curve, is significantly lower than in the experiments. This suggests a minor cohesive zone damage during the insert cycle. Here, the CZM uses the cohesive strength value provided by the BJ experiments (as described in Section 3.3). The value seems to be small for the insert cycle's CZM analysis because nonlinear behaviour occurs early, long before the maximum force of the insert cycle is reached. The small cohesive strength value also results in a significantly large cohesive zone (Eq. (11)) when compared to the relatively short cohesive zone provided by the cohesive strength value used in the combined method.

The combined method is able to provide a nonlinear force-displacement curve with close-to-correct maximum force, in contrast to the two-phase VCCT

simulation. Naturally, VCCT analysis does not lead to any nonlinearity before the crack onset because no interface degradation adjacent to the crack tip exists in the analysis. The slope of the VCCT unloading curve is lower than the slope of the curve provided by the combined method, which refers to a longer crack produced by the VCCT method. This indicates that the crack onset resistance of the combined model is higher than the crack resistance of the VCCT model. The slope of the unloading curve provided by the single-phase CZM method is the same as the slope provided by the combined method. This means that both models provide a similar crack length.

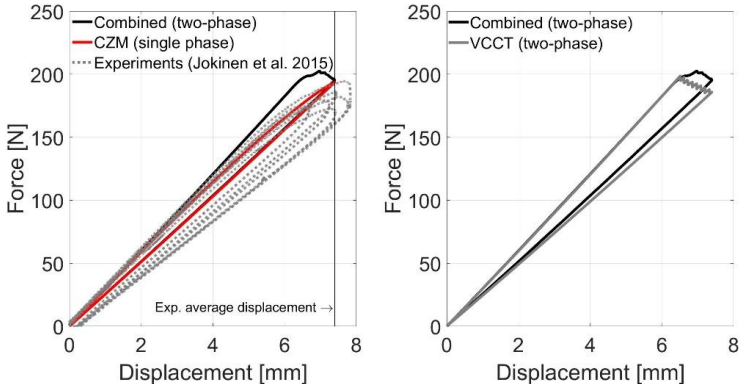


**Figure 23.** Experimental and simulation results of the DCB test insert cycle [P3].

### Crack propagation

One big challenge in numerically combining two fracture phases is the transition between the phases. In the combined method, the analysis method is changed from the CZM to the VCCT based on the procedure shown in Section 3.3. In the CZM analysis region, cohesive elements are attached to the interface using the tie constraint. The VCCT analysis region is defined to start from the nodal point following the CZM element region. In the transition region (element), no VCCT or CZM are modelled (Figure 15) in order to avoid an overconstrained situation. This setting does not provide a pre-existing crack before the CZM zone debonding when a linear shape function element is used.

The force-displacement curves provided by the combined method for the insert and precrack cycles are shown in Figure 24. The curves show a smooth transition between the cycles. This is a significant result for a simulation that is modelling a fracture with two separate methods. The smoothness indicates that the combined method is applicable in the studied case from the numerical point of view. In general, the transition could lead to crack-arresting behaviour, which is not the case here. Thus, the method is feasible for modelling the whole DCB experiment where crack nucleation and propagation phenomena are clearly divided into two tests.

Figure 24 also indicates that the combined method with its VCCT region provides a similar response for the crack propagation phase as did the experiments and the single-phase CZM model. The similarity of the curves is an in-

teresting finding, meaning that the combined method improves the onset phase simulation but not at the cost of the simulation accuracy of the propagation phase.

A challenge related to the applied parameters in the two-phase CZM analysis was also observed. In the studied case, the cohesive strength of the propagation model was smaller than the cohesive strength of the nucleation model. This led to a physically infeasible situation where element degradation occurred in the propagation phase ahead of the crack tip.

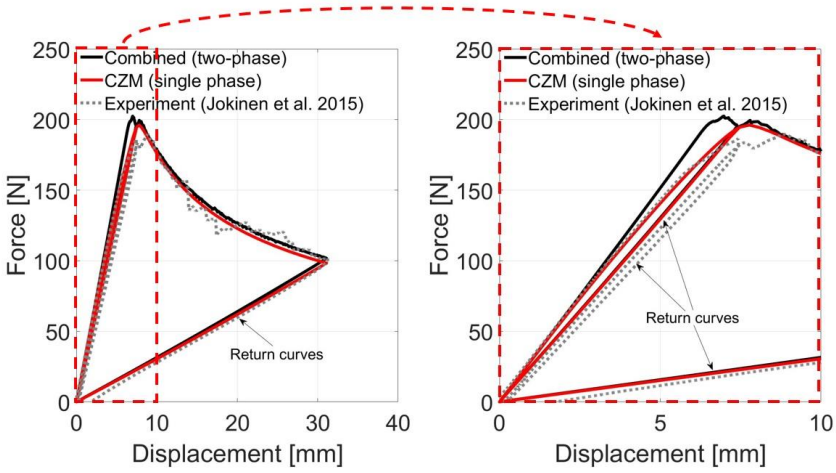


**Figure 24.** The transition between the onset and propagation phases [P3].

Numerical methods using separate techniques (models) for describing crack nucleation and propagation phases are scarce in the current literature. Carrere et al. (2015) studied micro-crack initiation using a stress criterion and macro-cracks using an energy criterion (i.e. by applying two criteria in one analysis). Other works related to crack nucleation and propagation analyses are focused on changing fracture parameter values along the propagation path. The evolution of a material's fracture toughness takes the form of an R-curve and has been described in the literature using the VCCT (Shokrieh, 2012) and the CZM (Gutkin, 2011). Davila et al. (2009) stated that linear CZM laws cannot describe toughening mechanisms that are shown as changes in the R-curve. For that reason, they developed laws superposing linear laws (Davila, 2009). The combined method introduced in this work has also been studied by Kanerva and Jokinen (2016). The performed literature survey did not reveal any other studies on a unified procedure combining two separate analysis methods.

The combined method allows separating two distinct fracture phases. Figures 23 and 24 indicate its applicability in simulating the crack nucleation and propagation phases. The method combines the advantages of the CZM and the VCCT, as highlighted in Table 8. The most important advantage is the ability to model the crack nucleation process, which in reality is a complex mixture of several micro-phenomena. The process has been studied by Basu et al. (2005).

**Table 8.** Assessment of the VCCT and CZM properties. Advantageous features of both methods are indicated with the blue colour fill (darker blue is more advantageous). The CZM-VCCT method combines these features. [P3]

| Property/method | CZM | VCCT |
|---|---|---|
| Nucleation | Stress-concentration initiates the fracture | A pre-existing singularity is necessary |
| Damage process zone | A traction-separation law defines softening (evolution), modelling the crack-tip development | No softening during self-similar propagation |
| Fracture modality | Mode division or an alternatively united deformation vector | Mode division |
| Material parameters | At minimum, one independent parameter is required in addition to fracture toughness | Fracture toughness |
| Nodal release | After reaching fracture toughness or separation | After virtual closure reaches fracture toughness |
| Plasticity at the crack tip | Explicitly valid | Difficult to validate |
| Sensitivity | Mesh sensitive | Minor mesh sensitivity |

## 4.4 Hybrid laminate

**Delamination onset**

Hybrid laminates are used to integrate some specific functionality into a structure. The studied laminate in Publications 4 and 5 [P4, P5] had a tungsten ply in the middle of stacked CFRP pre-preg layers. The target of the tungsten ply is to improve the radiation protection of the laminate. These laminates are used, for example, in space applications like satellite electronics enclosures. The challenge of the tungsten-CFRP hybrid laminate is the low adhesion between different plies (Kanerva, 2015b). Due to their de-adhesion tendency, delamination onset and propagation in the laminate were studied in Publications 4 and 5 [P4, P5]. The studied structure was a CLS specimen, as described in Section 3.4.

The delamination analysis of a hybrid laminate is complex when compared to analyses of conventional laminates. Layers of such a laminate have a mismatch in stiffness properties, which can lead to damage onset and growth at free edges. In the configuration of the studied hybrid laminate, the critical plane is the bi-material interface. Such an interface is a special case where the computed mixed-mode ratio (provided by the VCCT) can be dependent on the element length (Krueger, 2002). In addition to mechanical loading, the case study included thermal loading (due to cooling after curing). In Publication 4 [P4], crack onset and propagation characteristics of the hybrid laminate were studied using the VCCT and the CZM. Finally, the applicability of the combined method introduced in Publication 3 [P3] was studied in Publication 5 [P5] using the CZM parameters determined in Publication 4 [P4].

**Residual stress effects on fracture**

The studied hybrid laminate configuration involved a bi-material interface between CFRP and tungsten layers. Nosier and Maleki (2008) stated that the elastic property mismatch between such adjacent layers will create a highly concentrated interlaminar stress field near free edges. The stress level may also be high when compared to the interface strength (Unger, 1998).

The analytical equation for the ERR at the crack tip of the CLS specimen (Eq. (17)) presumes a one-dimensional crack (in a two-dimensional model) and neglects residual stresses. This limits the use of the equation. The VCCT is able to determine ERR values accounting for all three dimensions and the model can include a thermal loading step. For that reason, the VCCT was used to compute mode-mixity values and ERR values corresponding to the crack onset loading. A VCCT analysis was performed with and without thermal loading. Analytical equations were applied to compute a reference ERR and mode-mixity values without thermal loading.

Table 9 presents analysis results from the crack tip. The 'average' VCCT analysis values are based on all the nodal points at the crack tip while the 'middle' values are the values at the middle nodal point. Without thermal loading, the difference between average and middle values is seen to be minor for both the ERR and mode-mixity. Three-dimensionality thus has an insignificant influence on the ERR without thermal loading. This was verified by the ERR distributions in the width direction. The difference between analytical- and VCCT-based ERR values is around ten percent. This indicates that the 2D analytical equation provides a good estimate for the ERR value at the crack tip when thermal loading is neglected. The mode-mixity values ($\psi$) provided by the analytical equation and FE analysis are also at a similar level without any consideration of thermal loading.

Table 9 further indicates that the VCCT simulation result is completely different when a thermal loading step representing a realistic cure cycle (cooling) is included in the simulation. The most distinctive difference can be found in the average ERR value and in the mode-mixity ($\psi$) at the middle nodal point. A larger difference of average ERR values when compared to middle ERR values indicates that the ERR difference is highest at the edges. The mode-mixity values ($\psi$) indicate a change due to thermal loading, a change towards mode I at the edge and towards mode II in the middle.

The target of the ERR analysis in terms of the thesis research was to define critical ERR values for the delamination onset and propagation analyses. It is important to note that the failure process of the studied hybrid interface is unstable and very sudden in reality. Thus, nucleation and propagation processes are difficult to separate and the damage behaviour is defined by the nucleation ('onset').

The critical ERR values should be defined uniquely and independently at the precrack location. The initial crack length in the hybrid laminate (in the CLS specimen configuration) did not have a major effect on the ERR value [P5]. The representative critical ERR values for modes I and II were taken from the middle nodal point based on the analysis results in Publication 4 [P4]. This

middle point was not sensitive to element dimensions or free-edge stresses. Theoretically, the middle point represents the plane strain assumption, which is typically used in FE analyses of beam-like specimens (and in respective analytical models).

**Table 9.** The ERR and mode-mixity values computed for a hybrid CLS specimen analytically and numerically using a VCCT simulation [P4].

| Thermal load, $\Delta T$ | $G_I+G_{II}$, analytical | $\|\psi\|$ analytical | $G_I+G_{II}$, FE middle | $G_I+G_{II}$, FE average | $\psi$, FE middle | $\psi$, FE average |
|---|---|---|---|---|---|---|
| 100 °C | n/a | n/a | 261 J/m² | 317 J/m² | 71.8 ° | 55.9 ° |
| 0 °C | 307 J/m² | 59.6 ° | 283 J/m² | 280 J/m² | 61.1 ° | 62.1 ° |

**Fracture propagation under residual stresses**

The ERR value provided by the VCCT at the middle nodal point when including thermal loading was used as the critical ERR value in the delamination propagation analysis. The intended temperature change in the simulation was 100 °C but this was not achieved because of the sudden failure with the thermal loading $\Delta T$ = 86 °C, resulting in numerical difficulties in the implicit solution procedure. The VCCT delamination growth pattern under partial thermal loading ($\Delta T$ = 86 °C) is shown in Figure 25. It clearly shows that delamination mostly propagates along the edges while the nodal connections remain in the central area. The simulated delamination propagation was unstable, that is, sudden, once the delamination onset occurred. The VCCT model had severe convergence problems because of the instability, which finally led to aborting the analysis. These problems might be avoided with an explicit code, which should be studied in future work.

It should be noted that the delamination onset could not be initiated directly from the edge and towards the middle line in the VCCT model because of the requirement for a pre-existing crack (i.e. the VCCT precrack was not modelled at the edge). Still, the delamination propagated in parallel to the edges – initiating from the original straight crack tip. Since crack onset and propagation occurred before the thermal loading step was completed, the external tensile loading could not be applied at all in the analysis. Similar behaviour, that is, debonding due to partial thermal loading, was not observed in the experiments. Thus, the VCCT provided an inappropriate crack propagation in the case of the hybrid CLS specimen under residual stresses. In other words, the applied VCCT model was not feasible for the hybrid CLS specimen analysis.

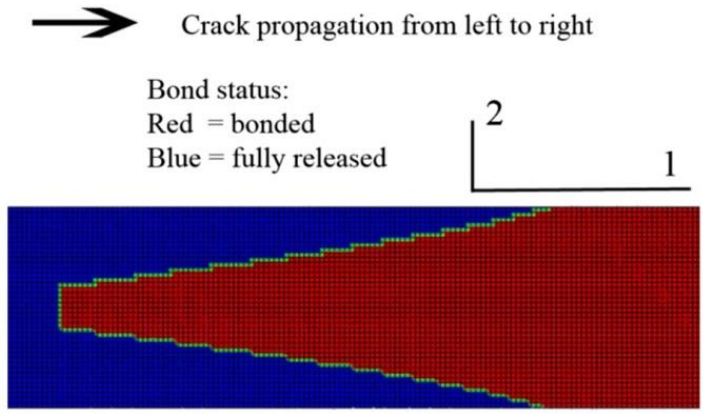


**Figure 25.** Delamination propagation patterns provided by the VCCT simulation for the hybrid CLS specimen under a partial thermal load ($\Delta T$ = 86 °C) [P5].

As a solution to the difficulties encountered in the VCCT analysis, the CZM was used for the CLS specimen crack growth analysis. In addition to the critical ERR values, a CZM analysis requires critical tractions and a stress criterion for defining the crack onset. The stress criterion was defined iteratively by comparing analysis data and experimental strain-versus-force curves. To simplify the iteration, ERR values provided by the VCCT analysis in the middle nodal point of the crack tip were chosen for the critical ERR values of the crack propagation criterion.

The CZM analyses were performed by applying full thermal loading before mechanical loading. The strain-force curves provided by the analyses with three sets of critical traction values are shown in Figure 26. The results indicate that the CZM is sensitive to the applied damage initiation criterion. This is explained by an unstable delamination growth, i.e. the delamination is growing significantly without major increase of loading. This behaviour is expectable since the ERR values at the crack tip are close to each other with different crack lengths. With the applied critical parameters $\tau_1$= 140 MPa and $\tau_2$= 240 MPa the analysis provides a proper correlation when compared to the experimental behaviour. The CZM simulation also proceeds correctly to the delamination propagation phase under the full thermal loading (100 °C) and mechanical load, as shown in Figure 27. According to the figure, the crack onset and propagation tendency is slightly higher at the edges when compared to the propagation at the centre (the middle line). The crack propagation pattern is drastically different, that is, less extensive and less concentrated to the edges, when compared to the pattern provided by the VCCT analysis (Figure 27 vs Figure 25). The difference can be explained with the difference in the interface stiffness of the models. The VCCT interface is almost rigid as provided by the contact formulation. On the other hand, CZM elements have a finite stiffness before damage onset and a cohesive zone before the complete damage of the elements. This has shown to relax singularities at the edge (Guillamet, 2016).

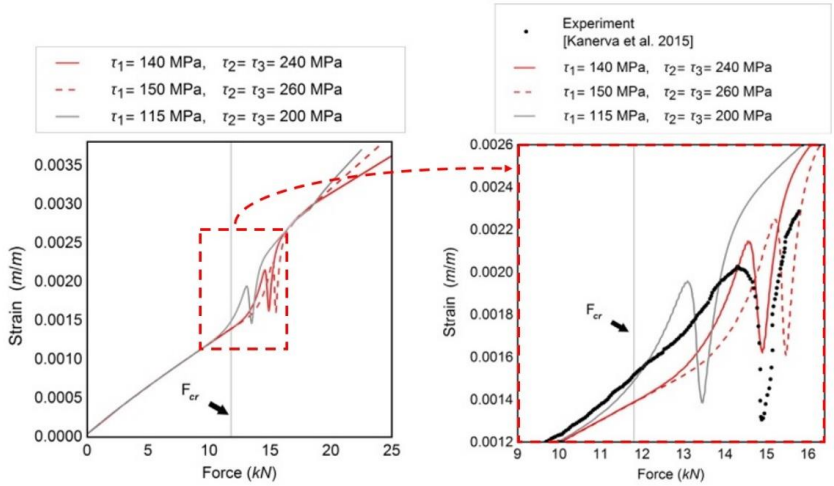


**Figure 26.** CLS test simulation performed with the CZM model using different traction values in the damage initiation criterion [P4].

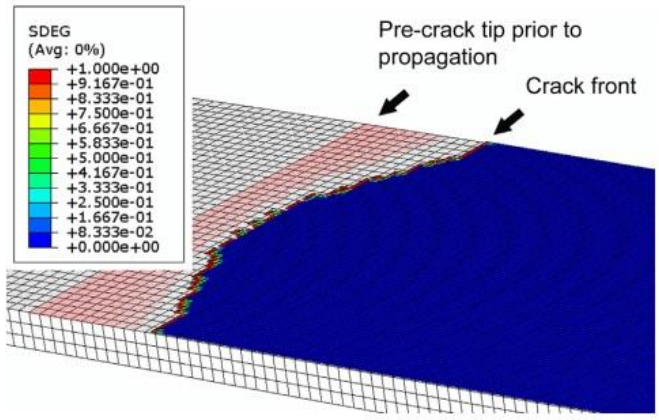


**Figure 27.** Interface damage state provided by the CZM model with full thermal loading (100 °C) and a mechanical load of 11 kN (the CZM damage parameter 0 is represents being bonded and 1 debonded) [P4].

The influence of the cohesive zone law on crack propagation has been widely studied in the current literature. Harper et al. (2012) stated that a wide range of interfacial stresses (such as the values in Fig. 26) can be used in analyses of simple fracture specimens with a precrack and when the crack tip's mixed mode ratio is *fixed*. The cohesive stress values are typically more realistic when the cohesive zone's length is short. In the study by Harper and Hallett (2008) they concluded that the global response of fracture specimens is relatively insensitive to interfacial stresses when studying events related to fracture mode I. In events related to fracture mode II, excessive material softening can exist ahead of the crack tip, which brings additional sensitivity to exact values (Harper, 2008). In the studied mixed-mode case [P4, P5], the analysis was sensitive to the interfacial stresses. This does not contradict the findings in the literature because the studied case was mode II dominant.

**Using the combined method for predicting damage onset and propagation under mixed-mode fracture and residual stresses**

In Publication 3 [P3] a fitting procedure was proposed for the combined method and its CZM parameters. The proposed procedure was studied under mode I crack-tip loading. In Publications 4 and 5 [P4, P5], the CLS specimen test did not include a separate 'insert cycle' where a natural crack front is formed. This differs from the DCB case of Publication 3 [P3] and, consequently, the transition point must be defined in a different way. Free edge stresses are typically limited to a small region but they incur high stress values close to the edge. For that reason, we assumed that the nucleation was fast and the related transition zone in the model was short including only one CZM element (in depth). Additionally, in contrast to Publication 3 [P3], the CLS specimen had a mixed-mode loading condition at the delamination tip. Because of the lack of a fitting procedure for the mixed-mode condition, the CZM parameters of the pure CZM model [P4] were directly used to define the nucleation process.

The combined CZM-VCCT method was mainly used for modelling the challenging crack onset. The delamination tip and possible debonding edges were modelled by using the CZM for the nucleation. The central region of the specimen was modelled by using the VCCT.

The results of the combined method analysis were compared to experimental results and to the pure CZM analysis data (Figure 28). After model configuration according to Publication 4 [P4], the combined method provided the delamination onset at the same force level as used in the experiment (and the pure CZM). In contrast to the pure CZM analysis, the combined method did not provide significant nonlinearity before the crack onset because the interface was mainly modelled using the VCCT which does not bring in interfacial compliance before bond failure. This explains the stiffer behaviour of the combined method model when compared to the pure CZM model described in Publication 4 [P4].

Also, the combined CZM-VCCT method did not lead to any delamination propagation (before a significant delamination growth). The results of the CZM analysis are thus more feasible than the results provided by the combined CZM-VCCT method in terms of nonlinearity. The results of the combined CZM-VCCT analysis are naturally affected by the CZM zone, which was only a single CZM element at the original crack tip. The obtained results suggest that the CZM nucleation zone in the combined CZM-VCCT model should be longer. The combined CZM-VCCT method, in the CLS case, was anyhow able to simulate the load level related to the significant delamination propagation.

The combined CZM-VCCT simulation of the CLS specimen testing was not completed due to convergence problems. The problems were caused by the unstable (VCCT) crack propagation and by the use of the implicit code. The implicit code was applied to allow a direct comparison between the combined CZM-VCCT analysis and the VCCT analysis of Publication 4 [P4]. The fact that the combined CZM-VCCT method, in this case, lacks nonlinearity in the re-

sults and leads to convergence problems, is a shortage. These issues are clearly a topic of future studies with a longer nucleation zone and with an explicit code.

Figure 29 presents results provided by the combined method in terms of the interface bond state after the thermal loading. According to Figure 29a, the delamination pattern (shown with a blue colour) is significantly different when compared to the pattern provided by the VCCT analysis (see, e.g. Fig. 25). The difference is due to the cohesive zone at the CZM region that limits the crack propagation caused by the thermal loading. The failed CZM elements are shown in Figure 29b with a red colour. The real nucleation region and the process zone that forms from it is difficult to experimentally specify (for mode II), but the fact that CZM halts the crack propagation at the specimen's edges indicates that the set cohesive zone leads to correct behaviour when compared to experiments.

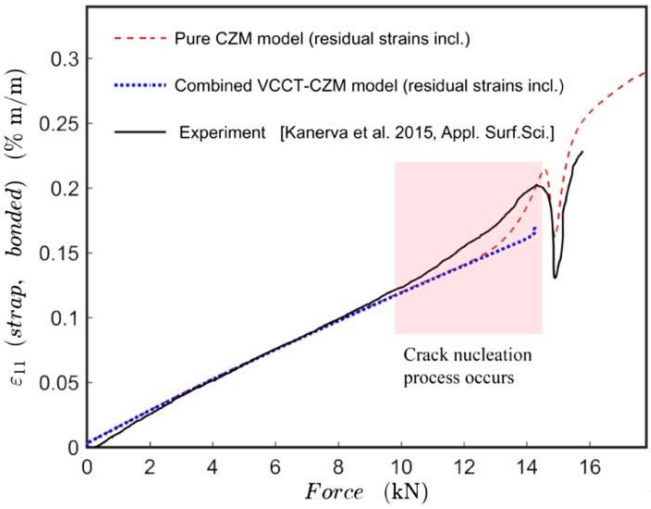


**Figure 28.** CLS test-related strain-force curves: the pure CZM model, the combined CZM-VCCT model and the experiment [P5].

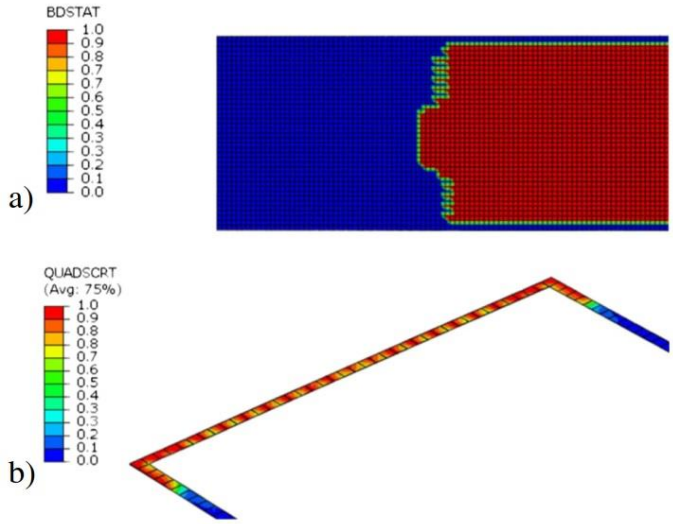


**Figure 29.** Crack front growth provided by the combined CZM-VCCT method after the thermal load cycle: (a) the VCCT region and (b) the CZM region. In the VCCT region, blue is represents being unbonded and red bonded; in the CZM region red refers to failure and blue to being intact [P5].

# 5. Conclusions

This work focuses on the applicability of the VCCT and CZM methods in the fracture analyses of structural delaminations and debondings. The work consists of four scientific studies that were performed in order to better understand the limitations of the methods and to find new types of applications for the methods.

## 5.1 Findings

The applicability of the VCCT in the analysis of an adhesively bonded joint was studied in Publication 1 [P1]. The VCCT was shown to be a feasible analysis method when there is plasticity in the adhesive of the studied DCB specimen. The main error in the analysis takes place at the beginning of crack propagation and is a consequence of the VCCT principle of collecting the reaction force and nodal displacement from different nodal points. The plastic deformation increases the difference in the stress states of these nodal points. The difference is most significant at the beginning of crack propagation. It evens up when the crack propagates and the formation of the plastic zone stabilises. The change is dependent on the plastic zone radius and on the applied element dimension.

The applicability of the VCCT analysis in the case of adherend nonlinearity was studied in Publication 2 [P2] by analysing the initial crack lengths of wedge peel test specimens with yielding adherends. Firstly, crack growth analyses were performed for aluminium and titanium (adherend) specimens in which the adherend behaviour was linear elastic. The VCCT analysis provided a feasible correlation with experimental results. In comparison, the VCCT provided slightly shorter crack lengths than the standard analytical equations (Plausinis, 1995).

The adherends of the studied steel specimens yielded in the test. The analytical equations fully neglect material nonlinearity, which naturally resulted in a considerable error in the evaluated initial crack length. The adherend load response was modelled in the VCCT analysis using a hypoelastic material model. The VCCT analysis provided a major improvement to the crack length prediction when compared to the analytical equations. However, the accuracy

decreased when the wedge thickness was increased (i.e. with increasing yielding of the adherends). This indicates that the performed VCCT simulation did not totally cover the nonlinear effects of the adherends.

Studies on FE-based methods using separate techniques for analysing crack nucleation and propagation phenomena are scarce in the current literature. The focus has been on fracture toughness evolution during crack propagation along the crack path (Shokrieh, 2012; Gutkin, 2011). The combined method generated in Publication 3 [P3] applied both the CZM and the VCCT in the crack nucleation and propagation simulation of a DCB specimen. In this combined method, the CZM provides the crack onset model and the VCCT provides the crack propagation modelling. The CZM of the combined method is able to simulate a crack nucleation process. This is not possible with the VCCT, which always requires a pre-existing crack for fracture simulation. In addition, the VCCT does not provide any stiffness degradation before the (nodal) bond failure, and it creates a rigid interface adjacent to the crack tip. The transition between the two separate methods in the combined method was shown to be smooth and properly sequential in terms of different crack phases. After the simulation of the crack onset, the crack propagation was efficiently simulated without any additional material parameters than fracture toughness. The crack propagation and the related specimen behaviour agreed well with the experimental data in the studied case (in the DCB test).

The VCCT and the CZM were also used in the challenging delamination analysis of hybrid CFRP/tungsten laminates described in Publications 4 and 5 [P4, P5]. The delamination fracture of a CLS specimen was studied under curing-related thermal loading and external mechanical loading. The bi-material interface between the CFRP and tungsten is complex because of the mismatch in the elastic properties of the layers which especially influences the fracture at laminate free-edges. Pure VCCT-related ERR distributions under the mechanical load, before delamination growth, were comparable with the analytical equation (Lai, 1996) when neglecting the thermal load. The addition of thermal loading significantly increased the mode I (i.e. peeling) loading at the edges. The delamination propagation analysis using the VCCT already provided overly extensive delamination growth during the thermal loading simulation. The growth was very unstable and the damage growth pattern did not correspond to the observations during experiments. The CZM was noted to be an appropriate method for analysing both loadings – presuming that the stress-based damage onset criterion is fitted properly. In Publication 4 [P4], it was shown that the CZM model's crack growth response was sensitive to the material values applied in the stress criterion.

Delamination of the hybrid laminate was finally analysed with the combined method generated in Publication 3 [P3]. The hybrid laminate testing (the CLS test) differed from the previously studied DCB test containing two separate test cycles. Therefore, the procedure described in Publication 3 [P3] was rede-

fined. CZM elements were modelled at the pre-crack tip through the specimen width and along the longitudinal specimen edges. The length of the CZM zone in the anticipated crack growth direction was one element which provided a shorter nucleation model zone than the previous DCB-fitted model. The combined method, in terms of parameters, was based on the procedure applied with the CZM model (a separate fitting procedure was not needed). The combined method predicted the failure load provided by the experiments. The simulation result differed from the CZM analysis result in that there was no major nonlinearity involved before the crack onset. The experiments show a similar nonlinearity than the CZM analysis. The obtained results indicate that the CZM model is more feasible for the studied case than the combined CZM-VCCT model. After onset, the combined model was stiffer than the CZM model because the VCCT was used in the crack propagation phase. Another interesting observation was that, when compared to the VCCT analysis result, a single CZM element at specimen edges of the CZM-VCCT model 'prevented' the delamination growth along the edges under the effects of thermal loading. The use of the combined CZM-VCCT method thus improved analysis results when compared to the VCCT analysis that, due to unstable delamination, could not be properly performed with the applied numerical parameters and implicit integration.

## 5.2 Future work

Typically, material nonlinearity is not considered in VCCT analyses. Based on the findings, the total restriction of nonlinearity is too limiting, but finding rules for the usage of nonlinear VCCT analyses demands more research work. In the current work, the adhesive was modelled using linear elastic-ideal plastic properties and self-similar crack propagation was achieved with small crack propagation. In the future, the effect of the applied material model should be studied in more detail. The reference case in the study was the DCB test with a pure mode I type loading of the bond. Future studies should also include mode II and mixed-mode (modes I/II) load cases in which the plastic region in the adhesive is larger.

The effect of the applied nonlinear material model should also be studied in analyses of bonded joints with yielding adherends. The material model applied in the current wedge peel test study does not cause permanent deformation, which may affect analysis results. The addition of the plastic deformation could provide more knowledge about the VCCT when the wedge peel test is analysed utilising the EDT. Another future research step could be to improve the measurement system of the wedge peel test. In the performed tests, the only measured quantity was the initial crack length, that is, the parameter evaluated with VCCT analyses. The comparison in terms of one quantity does not allow verification of the model's stiffness for example. The possibility of measuring the force of the wedge would be an improvement. Another improvement could be the utilisation of digital image correlation (Sargent,

2005), which would provide a full displacement field for the wedge and the specimen.

In future, the CZM-VCCT method should further be tested to find out how the applied nucleation and transition zone parameters affect its performance. The finite element mesh influence should also be covered in future studies. These studies should be performed to the extent that clear guidelines for the application of the CZM-VCCT methodology can be given. The applicability of the method should also be studied with different adhesives and adherends, and fracture property dependence on the FE mesh should be covered. The method development should be continued towards mixed-mode cases. The first practical case was already the CLS specimen analysis. For a realistic definition of the transition location, detailed fracture surface studies should be performed. The final target in the development of the combined method could be a capability to simulate realistic multi-damage cases in which different crack propagation routes are possible.

Residual stresses can have a significant effect on the structural performance of composite laminates and bonded repairs. For that reason, the use of the VCCT in analyses of hybrid laminates under thermal loading is a topic of interest. A target of further studies could concern revealing the reason for the poor performance of the VCCT in the current CLS specimen study, that is to say, whether the case was unique because of the bi-material interface or due to boundary conditions. The experienced instability of the analysis could be prevented using an explicit solver, which was not applied in this thesis.

# References


Abaqus (2014). Abaqus Analysis User's Manual, Abaqus 6.14 Documentation, Simulia.

Abaqus (2017a). Abaqus Analysis User's Manual, Abaqus 2017 Documentation, Simulia.

Abaqus (2017b). Abaqus Theory Manual, Abaqus 2017 Documentation, Simulia.

Agrawal, A., Karlsson, A. M. (2006). Obtaining mode mixity for a bimaterial interface crack using the virtual crack closure technique, Int J Fracture, 141, 75–98.

Alderliesten, R. C. (2009). Damage tolerance of bonded aircraft structures, Int J Fatique, 31, 1024–1030.

Alfano, G. (2006). On the influence of the shape of the interface law on the application of cohesive-zone models, Compos Sci Technol, 66, 723–730.

Alfano, M., Furgiuele, F., Leonardi, A., Maletta, C., Paulino, G. H. (2009). Mode I fracture of adhesive joints using tailored cohesive zone models, Int J Fracture, 157, 193–204.

Anyfantis, K. N., Berggreen, C. (2014). Characterizing and modelling brittle bimaterial interfaces subjected to shear, Appl Compos Mater, 21, 905–919.

Barenblatt, G. I. (1962). The mathematical theory of equilibrium cracks formed in brittle fracture, Adv Appl Mech, 7, 55–129.

Beuth, J. (1996). Separation of crack extension modes in orthotropic delamination models, Int J Fract, 77, 305–321.

Bonhomme, J., Argüelles, A., Viña, J., Viña, I. (2009). Numerical and experimental validation of computational models for mode I composite fracture failure, Comp Mat Sci, 45, 993–998.

Camacho, G. T., Ortiz, M. (1996). Computational modelling of impact damage in brittle materials, Int J Solids Structures, 33, 2899–2938.

Campilho, R. D. S. G., de Moura, M. F. S. F., Domingues, J. J. M. S. (2008). Using a cohesive damage model to predict the tensile behaviour of CFRP single-strap repairs, Int J Solids Struct, 45, 1497–1512.

Campilho, R. D. S. G., de Moura, M. F. S. F., Domingues, J.J.M.S. (2009). Numerical prediction on the tensile residual strength of repaired CFRP under different geometric changes, Int J Adhes Adhes, 29, 195–205.

Campilho, R. D. S. G., Banea, M. D., Neto, J. A. B. P., Da Silva, L. F. M. (2013). Modelling adhesive joints with cohesive zone models: effect of the cohesive law shape of the adhesive layer, Int J Adhes Adhes, 44, 48–56.

Carrere, N., Martin, E., Leguillon, D. (2015). Comparison between models based on a coupled criterion for the prediction of the failure of adhesively bonded joints, Eng Fract Mech, 138, 185–201.

Carvalho, U. T. F., Campilho, R. D. S. G. (2017). Validation of pure tensile and shear cohesive laws obtained by the direct method with single-lap joints, Int J Adhes Adhes, 77, 41–50.

Chen, C.-C., Linzell, D. G. (2010). Modeling end notched flexure tests to establish cohesive element Mode II fracture parameters, Eng Fract Mech, 77, 1338–1347.
Davila, C. G., Rose, C. A., Camanho, P. P. (2009). A procedure for superposing linear cohesive laws to represent multiple damage mechanisms in the fracture of composites, Int J Fract, 158, 211–223.
Dugdale, D. S. (1960). Yielding of steel sheets containing slits, J Mech Phys Solids, 8, 100–104.
Fan, C., Ben Jar, P.-Y., Roger Cheng, J. J. (2007). Prediction of energy release rates for crack growth using FEM-based energy derivative technique, Eng Fract Mech, 74, 1243–1254.
Fawaz, S. A. (1998). Application of the virtual crack closure technique to calculate stress intensity factors for through cracks with an elliptical crack front, Eng Fract Mech, 59, 327–342.
Fawaz, S. A. (1999). Stress intensity factor for part-elliptical through cracks, Eng Fract Mech, 63, 209–226.
Feraren, P., Jensen, H. M. (2004). Cohesive zone modelling of interface fracture near flaws in adhesive joints, Eng Fract Mech, 71, 2125–2142.
Ferracin, T., Landis, C. M., Delannay, F., Pardoen, T. (2003). On the determination of the cohesive zone properties of an adhesive layer from the analysis of the wedge-peel test, Int J Solids Struct, 40, 2889-2904.
Freed, Y., Banks-Sills, L. (2008). A new cohesive zone model for mixed mode interface fracture in bimaterials, Eng Fract Mech, 75, 4583–4593.
Glaessgen, E. H., Reeder, J. R., Sleight, D. W., Wang, J. T., Raju, I. S., Harris, C. E. (2005). Debonding failure of sandwich-composite cryogenic fuel tank with internal core pressure, J Spacecraft Rockets, 42, 613–627.
Goh, J. Y., Georgiadis, S., Orifici, A. C., Wang, C. H. (2013). Effects of bondline flaws on the damage tolerance of composite scarf joints, Compos Part A-Appl S, 55, 110–119.
Goland, M., Reissner, E. (1944). The stresses in cemented joints, J Appl Mech, 11, A-17–A27.
Goswami, S., Becker, W. (2001). The effect of facesheet/core delamination in sandwich structures under transverse loading, Compos Struct, 54, 515–521.
Goyal, V. K., Jaunky, N. R., Johnson, E. R., Ambur, D. R. (2004). Intralaminar and interlaminar progressive failure analyses of composite panels with circular cutouts, Compos Struct, 64, 91–105.
Grady, J. (1992). Fracture toughness testing of polymer matrix composites, NASA technical report, NASA-TP-3199.
Guillamet, G., Turon, A., Costa, J., Linde, P. (2016). A quick procedure to predict free-edge delamination in thin-ply laminates under tension, Eng Fract Mech, 168, 28–39.
Gustafson, P. A., Waas, A. M. (2009). The influence of adhesive constitutive parameters in cohesive zone finite element models of adhesively bonded joints, Int J Solids Struct, 46, 2201–2215.
Gutkin, R., Laffan, M. L., Pinho, S. T., Robinson, P., Curtis, P. T. (2011). Modelling the R-curve effect and its specimen-dependence, Int J Sol Struct, 48, 1767–1777.
Hadavinia, H., Kawashita, L., Kinloch, A. J., Moore, D. R., Williams, J. G. (2006). A numerical analysis of the elastic-plastic peel test, Eng Fract Mech, 73, 2324–2335.
Harper, P. W., Hallett, S. R. (2008). Cohesive zone length in numerical simulations of composite delamination, Eng Fract Mech, 75, 4774–4792.

Harper, P. W., Sun, L., Hallett, S. R. (2012). A study on the influence of the cohesive zone interface element strength parameters on mixed mode behaviour, Compos Part A-Appl S. 43, 722–734.

Hart-Smith, L. J. (1973). Adhesive-bonded single-lap joints. NASA contractor report, NASA-CR-112236.

Higgins, A. (2000). Adhesive bonding of aircraft structures, Int J Adhes Adhes, 20, 367–376.

Hirsch, F., Kästner, M. (2017). Microscale simulation of adhesive and cohesive failure in rough interfaces, Eng Fract Mech, 178, 416–432.

Ishai, O., Rosenthal, H., Sela, N., Drukker, E. (1988). Effect of selective adhesive interleaving on interlaminar fracture toughness of graphite/epoxy composite laminates, Composites, 19, 49–54.

ISO. (1987). Adhesives - Determination of Tensile Strength of Butt Joints, ISO 6922, International standard, modified.

ISO. (2001). Fibre-reinforced plastic composites – Determination of Mode I interlaminar fracture toughness, GIC, for unidirectionally reinforced materials, ISO 15024, International standard.

ISO. (2009). Adhesives – Determination of the Mode 1 adhesive fracture energy of structural adhesive joints using double cantilever beam and tapered double cantilever beam specimens, ISO 25217, International standard.

Jape, S., Baxevanis, T., Lagoudas, D. C. (2016). Stable crack growth during thermal actuation of shape memory alloys, Shape Memory and Superelasticity, 2, 104–113.

Jiang, Z., Wan, S., Zhong, Z., Li, S., Shen, K. (2015). Effect of curved delamination front on mode-I fracture toughness of adhesively bonded joints, Eng Fract Mech, 138, 73–91.

Jokinen, J., Wallin, M. (2015a). The Effect of Numerical Parameters on Debond Analyses Using VCCT in Abaqus, Nafems Nordic Seminar: Simulating composite materials and structures, 17–18 November, Stockholm.

Jokinen, J., Wallin, M., Saarela, O. (2015b). Delamination Analysis of Trailing Edge Flap, ICAF 2015 (International Committee on Aeronautical Fatigue and Structural Integrity) symposium, Helsinki.

Jokinen, J., Kanerva, M. (2017). Crack Onset Analysis of Adhesives for the CZM-VCCT Method, XIV International Conference on Computational Plasticity (COMPLAS 2017), Barcelona.

Kanerva, M., Jokinen, J., Sarlin, E., Saarela, O. (2013). Crack propagation under mode II dominance at stainless steel–epoxy interfaces with residual stresses and micro-scale roughness, Int J Solids Structures, 50, 3399–3405.

Kanerva, M., Johansson, L.-S., Campbell, J. M., Revitzer, H., Sarlin, E., Brander, T., Saarela, O. (2015a). Hydrofluoric-nitric-suplhuric-acid surface treatment of tungsten for carbon fibre-reinforced composite hybrids in space applications, Appl Surf Sci, 328, 418–427.

Kanerva, M., Jokinen, J., Antunes, P., Wallin, M., Brander, T., Saarela, O. (2015b). Acceptance Testing of Tungsten-CFRP Laminate Interfaces for Satellite Enclosures, International Conference on Composite Materials, 19–24 July, Copenhagen.

Kanerva, M., Jokinen, J. (2016). The effect of computational parameters on the performance of a combined CZM-VCCT Method, 29th Nordic Seminar on Computational Mechanics NSCM-29, Gothenburg.

Khoshravan, M., Mehrabadi, F. A. (2012). Fracture analysis in adhesive composite material/aluminium joints under mode-I loading: experimental and numerical approaches, Int J Adhes Adhes, 39, 8–14.
Krueger, R. (2002). The virtual crack closure technique: History, approach and applications, NASA contractor report, NASA-CR-2002-211628.
Krueger R. (2008). An approach to assess delamination propagation simulation capabilities in commercial finite element codes, NASA technical memorandum, NASA-TM-2008-215123.
Krueger, R., Ratcliffe, J. G., Minguet, P. J. (2009). Panel stiffener debonding analysis using a shell/3D modeling technique, Compos Sci Technol, 69, 2352–2362.
Lai Y.-H., Rakestraw, M. D., Dillard, D. A. (1996). The cracked lap shear specimen revisited – A closed form solution, Int J Solids Struct, 33, 1725–1743.
Lindgren, M., Bergman, G., Kakkonen, M., Lehtonen, M., Jokinen, J., Wallin, M., Saarela, O., Vuorinen, J. (2016). Failure analysis of a leaching reactor made of glass-fiber reinforced plastic, Eng Fail Anal, 60, 117–136.
Liu, P. F., Zheng, J. Y. (2010). Recent developments on damage modeling and finite element analysis for composite laminates: A review, Mater Design, 31, 3825–3834.
Marannano, G. V., Mistretta, L., Cirello, A., Pasta, S. (2008). Crack growth analysis at adhesive–adherent interface in bonded joints under mixed mode I/II, Eng Fract Mech, 75, 5122–5133.
Martiny, Ph. Lani, F., Kinloch, A. J., Pardoen, T. (2008). Numerical analysis of the energy contributions in peel tests: A steady-state multilevel finite element approach, Int J Adhes Adhes, 28, 222–236.
Meo, M., Thieulot, E. (2005). Delamination modelling in a double cantilever beam, Compos Struct, 71, 429–434.
Mikulik, Z., Kelly, D. W., Gangadhara Prusty, B., Thomson, R. S. (2008). Prediction of initiation and growth of single level delaminations in a transversely loaded composite specimen using fracture mechanics, Int J Fract, 149, 119–141.
MIL-HDBK-5J (2003). Metallic materials and elements for aerospace vehicle structures, Department of Defense Handbook.
Nguyen, V. P., Nguyen-Xuan, H. (2013). High-order B-splines based finite elements for delamination analysis of laminated composites, Compos Struct, 102, 261–275.
Nosier, A., Maleki, M. (2008). Free-edge stresses in general composite laminates, Int J Mech Sci, 50, 1435–1447.
O'Brien, K. (1981). Characterization of delamination onset and growth in a composite laminate, NASA technical memorandum, NASA-TM-81940.
Orifici, A. C., Krueger, R. (2012). Benchmark assessment of automated delamination propagation capabilities in finite element codes for static loading, Finite Elem Anal Des, 54, 28–36.
Pardoen, T., Ferracin, T., Landis, C. M., Delannay, F. (2005). Constraint effects in adhesive joint fracture, J Mech Phys Solids, 53, 1951–1983.
Pietropaoli E., Riccio A. (2010). On the robustness of finite element procedures based on virtual crack closure technique and fail release approach for delamination growth phenomena. Definition and assessment of a novel methodology, Compos Sci Technol, 70, 1288–1300.
Plausinis, D., Spelt, J. K. (1995). Designing for time dependent crack growth in adhesive joints, Int J Adhes Adhes, 15, 143–154.
Pärnänen, T., Vänttinen, A., Kanerva, M., Jokinen, J., Saarela, O. (2016). The effects of debonding on the low-velocity impact response of steel-CFRP fibre metal laminates, Appl Compos Mater, 23, 1151–1166.

Raju, I. S. (1986). Simple formulas for strain-energy release rates with higher order and singular finite elements, NASA contractor report, NASA-CR-178186.
Raju, I. S., Crews Jr., J. H., Aminpour, M. A. (1987). Convergence of strain energy release rate components for edge-delaminated composite laminates, NASA technical memorandum, NASA-TM-89135.
Rice, J. R. (1968). A path independent integral and the approximate analysis of strain concentration by notches and cracks, J Appl Mech, 35, 379–386.
Rybicki, E. F. and Kanninen M. F. (1977). A finite element calculation of stress intensity factors by a modified crack closure integral, Eng Fract Mech, 9, 931–938.
Salpekar, S. A., O'Brien, T. K., Shivakumar, K. N. (1996). Analysis of local delaminations caused by angle ply matrix cracks, J Compos Mater, 30, 418–440.
Sargent, J. P. (2005). Durability studies for aerospace applications using peel and wedge tests, Int J Adhes Adhes, 25, 247–256.
Shet, C., Chandra, N. (2002). Analysis of energy balance when using cohesive zone models to simulate fracture process, J Eng Mater-T Asme, 124, 440–450.
Shokrieh, M. M., Rajabpour-Shirazi, H., Heidari-Rarani M., Haghpanahi, M. (2012). Simulation of mode I delamination propagation in multidirectional composites with R-curve effects using VCCT method, Comp Mater Sci, 65, 66–73.
Soutis, C. (2005). Fibre reinforced composites in aircraft construction, Prog Aerosp Sci, 41, 143–151.
Stone, M. H., Peet, T. (1980). Evaluation of the wedge cleavage test for assessment of durability of adhesive bonded joints (epoxy resin), Royal Aircraft Establishment, Technical Memorandum, p. 24.
Sun, C. T., Manoharan, M. G. (1989). Strain energy release rates of an interfacial crack between two orthotropic solids, J Compos Mater, 23, 460–478.
Sun, C. T., Wang C. Y. (2002). A new look at energy release rate in fracture mechanics, Int J Fract 113, 295–307.
Suo, Z., Hutchinson, J. W. (1990). Interface crack between two elastic layers, Int J Fract, 43, 1–18.
Tawk, I., Navarro, P., Ferrero, J.-F., Barrau, J.-J., Abdullah, E. (2010). Composite delamination modelling using a multi-layered solid element, Compos Sci Technol, 70, 207–214.
Turon, A. (2006). Simulation of delamination in composites under quasi-static and fatigue loading using cohesive zone models, PhD thesis, Universitat de Girona.
Turon, A., Dávila, C. G., Camanho, P. P., Costa, J. (2007). An engineering solution for mesh size effects in the simulation of delamination using cohesive zone models, Eng Fract Mech, 74, 1665–1682.
Unger, W. J., Hansen, J. S. (1998). A method to predict the effect of thermal residual stresses on the free-edge delamination behavior of fibre reinforced composite laminates, J Compos Mater, 32, 431–459.
Valoroso, N., Sessa, S., Lepore, M., Cricri, G. (2013). Identification of mode-I cohesive parameters for bonded interfaces based on DCB test, Eng Fract Mech, 104, 56–79.
Valvo, P. S. (2012). A revised virtual crack closure technique for physically consistent fracture mode partitioning, Int J Fract, 173, 1–20.
Volokh, K. Y. (2004). Comparison between cohesive zone models, Commun Numer Meth En, 20, 845–856.
Wang, J. T., Raju, I. S. (1996). Strain energy release rate formulae for skin-stiffener debond modeled with plate elements, Eng Fract Mech, 54, 211–228.

Wilkins, D. (1981). A comparison of the delamination and environmental resistance of a graphite-epoxy and a graphite-bismaleimide, Tech Rep NAV-GD-0037 (AD-A1122474), Naval Air Systems Command, USA.

Xiao, T., Liao, R.-D., Zuo, Z.-X. (2009). Computations of energy release rate under monotonic and cyclic loading conditions, Comp Mater Sci, 46, 694–699.

Xie, D., Waas, A. M., Shahwan, K. W., Schroeder, J. A., Boeman, R. G. (2005a). Fracture criterion for kinking cracks in a tri-material adhesively bonded joint under mixed mode loading, Eng Fract Mech, 72, 2487–2504.

Xie, D., Chung, J., Waas, A. M., Shahwan, K. W., Schroeder, J. A., Boeman, R. G., Kunc, V., Klett, L. B. (2005b). Failure analysis of adhesively bonded structures: from coupon level data to structural level predictions and verification, Int J Fract, 134, 231–250.

Xie, D., Waas, A. M. (2006). Discrete cohesive zone model for mixed-mode fracture using finite element models, Eng Fract Mech, 73, 1783–1796.

Xu, Y., Li, X., Wang, X., Liang, L. (2014). Inverse parameter identification of cohesive zone mode for simulating mixed-mode crack propagation, Int J Solids Struct, 51, 2400–2410.

Xu, X., Needleman, A. (1993). Void nucleation by inclusion debonding in a crystal matrix, Modelling Simul Mater Sci Eng, 1, 111–132.

Yang, Q. D., Thouless, M. D., Ward, S. M. (1999). Numerical simulations of adhesively-bonded beams failing with extensive plastic deformation, J Mech Phys Solids, 47, 1337–1353.

Yang, C., Sun, W., Tomblin, J. S., Smeltzer, S. S. (2007). A semi-analytical method for determining the strain energy release rate of cracks in adhesively-bonded single-lap composite joints, J Compos Mater, 41, 1579–1602.

Yang, Q., Cox, B. (2005). Cohesive models for damage evolution in laminated composites, Int J Fract, 133, 107–137.

Zou, Z., Reid, S. R., Li, S., Soden, P. D. (2002). Modelling interlaminar and intralaminar damage in filament-wound pipes under quasi-static indentation, J Compos Mater, 36, 477–499.

Aalto-DD 212/2019

ISBN 978-952-60-8824-2 (printed)
ISBN 978-952-60-8825-9 (pdf)
ISSN 1799-4934 (printed)
ISSN 1799-4942 (pdf)

**Aalto University**
**School of Engineering**
**Department of Mechanical Engineering**
**www.aalto.fi**

**BUSINESS + ECONOMY**

**ART + DESIGN + ARCHITECTURE**

**SCIENCE + TECHNOLOGY**

**CROSSOVER**

**DOCTORAL DISSERTATIONS**